

**Studies on Non-invasive Left Ventricle Function Evaluation in  
Hypertensive and Uremic Cardiomyopathy Rat Model**

高血圧性心筋症および尿毒症性心筋症のラットモデルにおける左心室機能の非侵襲  
的評価に関する研究

**2021**

**The United Graduate School of Veterinary Science,  
Gifu University  
(Tokyo University of Agriculture and Technology)**

**Ma Danfu**

# Index

Abbreviation .....	- 5 -
GENERAL INTRODUCTION .....	- 6 -
Chapter 1 Exploring the principle of intraventricular pressure gradients sampling.....	- 13 -
1.1 Introduction .....	- 14 -
1.2 Materials and methods .....	- 15 -
1.2.1 Research design .....	- 15 -
1.2.2 Animal welfare .....	- 16 -
1.2.3 Induction of left ventricle hypertrophy .....	- 16 -
1.2.4 Measurement of blood pressure .....	- 17 -
1.2.5 Anesthesia protocol.....	- 17 -
1.2.6 Conventional echocardiographic assessment.....	- 18 -
1.2.7 Tissue Doppler imaging.....	- 19 -
1.2.8 Colour-M-mode-echocardiography for assessment of IVPG.....	- 19 -
1.2.9 Statistical analysis.....	- 20 -
1.3 Results .....	- 21 -
1.3.1 Conventional echocardiography .....	- 21 -
1.3.2 Tissue Doppler imaging.....	- 21 -
1.3.3 IVPG measurements .....	- 21 -
1.3.4 Pearson's Correlations test of the novel echocardiography .....	- 22 -
1.4 Discussion.....	- 23 -
1.5 Limitation .....	- 24 -

1.6 Clinical implication .....	- 25 -
1.7 Conclusion .....	- 25 -
Chapter 2 Investigation of the cardiac function in pressure-overload model.....	- 35 -
2.1 Introduction .....	- 36 -
2.3 Materials and methods .....	- 38 -
2.3.1 Animal .....	- 38 -
2.3.2 Induction of hypertensive cardiomyopathy.....	- 39 -
2.3.3 Research design .....	- 39 -
2.3.4 Echocardiographic measurements .....	- 40 -
2.3.5 Tissue Doppler imaging.....	- 41 -
2.3.6 Colour M-mode echocardiography derived intraventricular pressure gradients .....	- 42 -
2.3.6 Blood pressure .....	- 42 -
2.3.7 Statistical analysis .....	- 43 -
2.4 Results .....	- 43 -
2.4.2 IVPG measurements .....	- 44 -
2.6 Limitation .....	- 49 -
2.7 Conclusion.....	- 49 -
Chapter 3 Cardiac function change during the development in the complex pressure and volume overload model.....	- 62 -
3.1 Introduction .....	- 63 -
3.2 Materials and Methods .....	- 65 -
3.2.1 Research design .....	- 65 -
3.2.2 Animal .....	- 66 -

3.2.3 Induction of uraemic cardiomyopathy .....	- 66 -
3.2.4 Sal B treatment .....	- 66 -
3.2.5 Echocardiography .....	- 67 -
3.2.6 Blood sampling.....	- 68 -
3.2.7 Statistical analysis.....	- 68 -
3.3 Results .....	- 68 -
3.4 Discussion.....	- 70 -
3.5 Limitation .....	- 73 -
3.6 Conclusion .....	- 73 -
General Conclusion .....	- 83 -
Study limitation .....	- 85 -
Acknowledgment.....	- 87 -
References .....	- 89 -

## Abbreviation

A	late mitral inflow (atrial systole)
a'	tissue velocity at late diastole
ANOVA	Analysis of Variance
ATP	adenosine triphosphate
B-mode	brightness mode
cAMP	cyclic adenosine monophosphate
CMME	colour M-mode echocardiography
CM	cardiomyopathy
CVDs	cardiovascular diseases
E	early mitral inflow
e'	tissue velocity at early diastole
EA-fusion	fused (E and A waves)
EA-half-separation	partial fused (E and A waves)
EA-separation	separated (E and A waves)
ECG	electrocardiograph
EF	ejection fraction
FS	fractional shortening
HF	heart failure
HR	heart rate
IL	interleukin
IVPD	intraventricular pressure difference
IVPG	intraventricular pressure gradient
IVSd	interventricular septal wall thickness at end-diastole
LA	left atrium
LV	left ventricle
LVIDd	left ventricular internal diameter at end-diastole
LVM	left ventricular mass
LVOT	left ventricular outflow tract
LVPWd	left ventricular posterior/lateral wall thickness at end-diastole
n	number
NAD <sup>+</sup>	nicotinamide adenine dinucleotide
NO	nitric oxide
p	probability of finding the observed results
RWT	relative wall thickness
s'	tissue velocity at systole
SBP	systolic blood pressure
Sham	placebo surgery
TDI	tissue Doppler imaging
TM- or M-mode	time-motion mode (or motion mode)

## **GENERAL INTRODUCTION**

Cardiovascular diseases (CVDs) are the disorder of the heart and blood vessels. In 2020, CVDs cost around 17.9 million lives (1), representing 31% of all global deaths. It was considered as the first cause of death globally, more people die from CVDs than from any other cause including cancer, pandemic infectious disease like 2.8 million by COVID-19. Premature death is one of the severe outcomes of CVDs, around 25% of CVDs death occurred in people under 70 years of age. Early detection and management dramatically decrease the mortality of CVDs.

CVDs are also popular in dogs, around 10% of dogs have CVDs in the United States. The majority CVDs in dogs have acquired diseases that mainly affect mitral, pulmonary, and aortic valves, while cardiomyopathy was also observed in some species(2). In cats, hypertrophic cardiomyopathy (HCM), characterized as the thickening of the septum or free wall, is the most commonly encountered disease. Approximately one-sixth of cats have HCM and the prevalence increased with age, which eventually developed into congestive heart failure, arterial thromboembolism, and sudden death (3, 4). Thus, CVDs are of key importance in the field of human and veterinary medicine.

Although patients would report syndrome-like angina pectoris and chest pain, some CVDs are still hard to diagnose without invasive catheterization (5). And early-stage CVDs are asymptomatic in animals and humans, pet owners and humans are hard to notice CVDs except for the annual examination. Because of the need for highly sensitive techniques in human CVDs diagnosis and the asymptomatic character of humans and animals, evaluation of cardiac function noninvasively becomes crucial as it provides early and accurate detection of CVDs. Besides, physicians and veterinarians rely on the evaluation of cardiac function to stage CVDs and prescribe medicine(4, 6). Quality of life and life expectancy could be promoted by early diagnosis and therapeutic intervention in congestive heart failure cases in human and veterinary medicine (7, 8).

Evaluation of cardiac function plays a crucial role in CVDs diagnosis and pathophysiological mechanism. There are two ways to evaluate cardiac function: invasive and non-invasive techniques. Although invasive catheterization is still the gold standard in imaging for coronary arteries and pressure assessment inside the ventricle and atrium (9), the laborious, unrepeatable, and highly invasive characters of catheterization limited its availability. Recently, as novel techniques developed progressively throughout the field of medicine and veterinary medicine, noninvasive visualizing techniques of the heart for the evaluation of cardiac function have become reality. Noninvasive techniques including magnetic resonance imaging computed tomography, and ultrasound become available in human and veterinary practice (10). Among these non-invasive techniques, echocardiography is considered the most useful and accurate technique, because it provides high-resolution images in real-time with quantitative assessment and it is more accessible than other techniques(11).

Although echocardiography has been considered as the basic examination method for noninvasive imaging, there was still some problem need to be explored(6). Conventional echocardiography is interfered with by many short-term factors including excitement and blood volume. Many veterinary and human patients are stressed because of the foreign environment and medical technicians during echocardiography examination and even the hydration status will interfere with the test, which eventually led to disturbance of echocardiography results(4, 12). For instance, the altered hydration status leads to changes in the echocardiography parameter in normal cats which results in an erroneous diagnosis of cardiomyopathy or covers its existence (13). To overcome these disadvantages of conventional echocardiography and provide direct diastolic function evaluation, scientists developed intraventricular pressure gradients.

Intraventricular pressure gradients have been described by Ling et al and Falsetti et al around 40 years ago, to evaluate the small pressure difference inside the LV during diastole



that drives blood from the LA to LV through the mitral valve (9, 14). The pressure difference is also termed diastolic suction force and is responsible for the early filling of the ventricle (E wave) at low mean LA pressure. The pressure difference was proved to promote inotropic stimulation and it was decreased after ischemia (15).

Measuring the pressure difference is rare because it could not gain from simple Doppler techniques. The difference occurred at the time of peak flow acceleration, rather than peak flow. Therefore, it cannot be calculated by the simplified Bernoulli equation. To solve this problem, scientists developed a new way to calculate intraventricular pressure differences (IVPD) from colour M-mode Doppler echocardiography (CMME) as shown in figure 1 (16, 17).

Yotti et al use the Euler equation, which is a differential version of the Bernoulli equation for pressure change along a streamline of flow, as shown below:

$$\frac{\partial p}{\partial s} = -\rho \left[ \frac{\partial v}{\partial t} + v \frac{\partial v}{\partial s} \right]$$

$V$ , three-component vector of local blood velocity;  $s$ , distance along the central streamline from the left atrium to left ventricle;  $\rho$ , Blood density,  $1.05 \text{ g/cm}^3$ ;  $\frac{\partial p}{\partial s}$ , the partial derivative of pressure concerning space;  $\frac{\partial v}{\partial t}$ , the partial derivative of velocity concerning time;  $\frac{\partial v}{\partial s}$ , the partial derivative of velocity concerning space (left atrium to left ventricle).

In this equation, scientists could gain pressure gradients with the velocity, space, and time along the streamline of flow, which could be provided by the color-m-mode-echocardiography (CMME). Then the smoothed velocity map was applied to the noise-magnifying partial derivatives, the misalignments error during this process was low enough to get the trustworthy pressure difference (18).

The intraventricular pressure gradients (IVPG) could be calculated by pressure difference by the following equation:

$$\text{Intraventricular pressure gradients} = \frac{\text{Intraventricular pressure difference}}{\text{length of the left ventricle}}$$

Because the IVPD was reported to positively correlate with the length of LV (19), the IVPG could avoid the effect of length of LV. *Tau*, the time constant of pressure decay, is the gold standard of diastolic function. IVPG was reported to negatively correlate with *tau* in humans (19). The augmentation in diastolic IVPG was observed with the preload increases. Invasive IVPG measurement not only requires multiple high-fidelity sensors but is also considered as not inappropriate for a clinical routine check for its laborious, unrepeatable, and highly invasive. Noninvasive IVPG derived by CMME was reported to well correlate with invasive IVPG, thus noninvasive IVPG by CMME was regarded as a promising technique in evaluating cardiac function (20).

IVPG enabled scientists to gain cardiac function noninvasively, thus it could provide an evaluation of cardiac function along with the time series. Although the invasive pressure-volume loop provides a more accurate evaluation of cardiac function (21), the invasiveness limited its repeated use to achieve the monitoring of cardiac function. Although Doppler E velocities sampled by conventional echocardiography are the most used indicator for hemodynamic function, it is not sufficient to assess diastolic function for the following reasons: first, the impact of preload to conventional echocardiography cannot be ignored (22). Second, conventional echocardiography owns inevitable demerit including angle-dependent, and reliance on geometrical assumptions(12). Third, conventional echocardiography cannot evaluate diastolic function directly and quantitatively. Therefore, for the first time, scientists could gain a comprehensive assessment of hemodynamic status noninvasively by advanced echocardiography technique——IVPG. IVPG helps scientists understand the pathophysiology

of CVDs and explore the treatment with a better outcome(23). Compare with invasive catheterization, IVPG provides more close monitoring of cardiac function with or without medication intervention for the first time. The pathophysiology exploring of CVDs will enter a new era by more accurate and timely monitoring. Although reports of IVPG in the rodent model were reported (24), close monitoring of cardiac function was not performed to explore the pathophysiology of CVDs. With further understanding of the pathophysiology of CVDs, physicians and veterinarians could have important insight into the management of CVDs, which eventually will improve the quality of life and life expectancy of humans and animals.

The primary purpose of this quantitative thesis is to develop a novel and sensitive echocardiographic measurement to gain an understanding of CVDs pathophysiology and evaluate the treatment effect of the medicine.

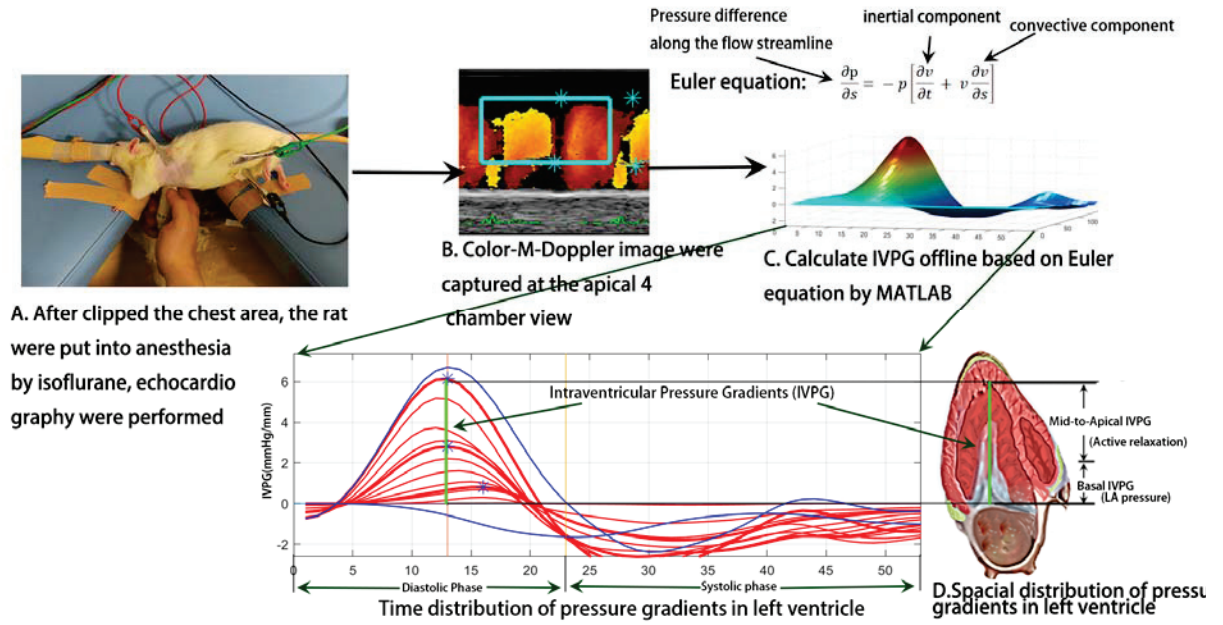


Figure 1. Analysis of intraventricular pressure gradients (IVPG). IVPG is calculated by using the Euler equation.

**Chapter 1**  
**Exploring the principle of intraventricular pressure gradients sampling**

## 1.1 Introduction

Evaluation of cardiac function is of the key importance of CVDs in diagnosis and exploring of pathophysiology. Conventional echocardiography was the most used technique to evaluate cardiac function noninvasively, but the defect of conventional echocardiography including easily be affected by short-term effects like heart rate, excitement, and mitral inflow pattern change that are hard to be neglected(25, 26). Conventional echocardiography uses the mitral inflow velocity graph to judge the diastolic function, which is indirect and challenging in some scenarios. For instance, it is difficult to estimate the filling pressure in patients with normal or preserved ejection fraction, because the status of myocardial relaxation cannot be clarified(27).

Also, diastolic dysfunction occurs before systolic dysfunction which means the diastolic function is a parameter more sensitive than systolic function in CVDs diagnosis(28, 29).

Thus, scientists developed intraventricular pressure gradients (IVPG), which create a suction force that drives the blood from the left atrium (LA) to the LV during early diastole(18). This mechanism plays a crucial role in diastole because the early diastole fills approximately 80% of the ventricle volume. Therefore, IVPG is considered a diastolic indicator *in vivo*. Noninvasive IVPG measurement from colour-M-mode-echocardiography (CMME) using the Euler equation is well correlated with the gold standard of diastolic function parameter *tau* which refers to the LV diastolic time constant (30-32). Moreover, IVPG can be used for serial assessment of diastolic function in healthy and hypertensive cardiomyopathy (HTN-CM) animals as well as humans from infant to adult (33, 34). Thus, IVPG could easily grade the HTN-CM patients using the diastolic function (33).

The cardiac cycle consists of the diastole and systole phases and the diastole is the phase that the heart refills with blood after the cardiac contraction (systole). The whole diastole

duration could be divided into three phases: the Doppler E wave for early rapid filling; an interval between flows for diastasis; and the Doppler A wave for late filing due to atrial systole. The effect of heart rate (HR) on the whole diastole duration is easy to understand because of known cellular physiology and kinematic cardiac modeling. When the HR is high, the average heartbeat decreased. Because the systole phase takes constant time, so the diastole duration was low in high HR. Scientists proved that the duration of the E wave and A wave is independent of the impact of HR when the HR increases (35). 100% increase in HR only generates 18% and 16% decrease in E and A-wave duration. Therefore, the diastasis was mainly diminished when the diastole duration is decreased. However, when the HR is elevated in CVDs, the diastasis even disappeared, the E and A wave may mix into only one wave: EA-fusion wave(Figure 1-1, A). The evaluation of cardiac function in the EA-fusion pattern by IVPG and traditional echocardiography is unknown.

The primary purpose of this study was to explore the pathophysiology of CVDs and to evaluate the effect of treatment. Due to lacking the principle of novel echocardiography sampling, I cannot gain accurate cardiac function by novel echocardiography techniques like IVPG. Therefore, the first chapter aimed to determine whether IVPG is affected by short-term effects like heart rate and mitral inflow patterns changes in the animal model.

## **1.2 Materials and methods**

### **1.2.1 Research design**

A total of 99 female Sprague Dawley rats purchased from Charles River Laboratory (Tokyo, Japan), 2.5 months age, and weighing 220-250 grams were included in this experiment. The study was approved by the Institutional Animal Care and Use Committee (ID: 31-36) dated

July 22, 2019. The Guide for the Care and Use of Laboratory Animals (1994) was followed during the execution of this experiment.

The HR was not controlled by the pacemaker in this experiment, as the pacemaker can only increase the heart rate and electrocardiography will be interfered with by the pacemaker. In the current group, rats were divided into different groups based on their mitral inflow pattern. Because the anesthesia was controlled equal to every rat, thus the mitral inflow pattern and heart rate were stable during the echocardiography, that short-term effect like excitement was excluded. This dividing system was more natural and scientific than artificially controlling the heart rate to producing different mitral inflow patterns and heart rates (31, 35).

### **1.2.2 Animal welfare**

The rats in this experiment received water and food *ad libitum* and were housed at 21°C under air-conditioning based on a 12-h light/dark cycle.

Although many rats were included in this study, some rats were used from another study that underwent aorta coarctation surgery and sham operation. These studies have the same experimental procedures but different objectives, and the Replace, Reduce, Refine principle of animal welfare and experimental design has been considered.

### **1.2.3 Induction of left ventricle hypertrophy**

An abdominal aorta coarctation operation was performed on 66 rats as previously described(36). Briefly, rats were injected with 40 mg/kg Pentobarbital sodium for anesthesia and, then put the rat dorsal recumbency under the operating microscope (Leica M60, Wetzlar, Germany). The abdominal aorta was explored by cotton swab and sutured with a 0.72 mm



diameter needle by 3-0 silk (Figure. 1-1. D). After checking the knot stability, I withdrew the needle and closed the incision after confirming the blood supply had returned to the hind limb without any cyanosis.

Also, the sham operation was performed as a control in the remaining 33 rats (Figure. 1-1. E), which indicates that the abdomen was opened and the infrarenal aorta was explored before suturing the incision. Measurement of blood pressure, conventional echocardiography, and CMME were performed 3 weeks after the operation in all rats. Aortic coarctation rats developed HTN-CM based on the existence of elevated left ventricle mass (LVM) and elevated blood pressure (37).

#### **1.2.4 Measurement of blood pressure**

The noninvasive blood pressure was sampled by the oscillometric method from the tail (BP monitor for rats, Muromachi, Japan) when the rat was put into a small cage to limit its movement. Three different sizes of cages and cuffs were used to suit rats from 140g to 800g. The consecutive measurement was performed 3 times at each sampling, the average of systemic systolic, diastolic, and mean arterial blood pressure was reported.

#### **1.2.5 Anesthesia protocol**

The following procedure was performed to prevent the effect of excitement on HR and keep the anesthesia effect to all rats were homogeneous. I choose isoflurane to induce and maintain the anesthesia because isoflurane owns has the cardioprotective effect and it was mainly metabolized by the lung (38, 39). 4% isoflurane with 1 L/min oxygen was used for the anesthesia induction. The rats will be passing the Stage 1 and 2 anesthesia stage based on

Guedel's classification, which means the rats will be analgesia and excited. When the rats reached the surgical anesthesia stage (stage 3), the eyelid, conjunctival, and swallow reflexes usually disappear in this phase (40). Then the rats were allowed to spontaneously breathe during 2.5% isoflurane for maintenance. The mandibular and maxilla were inserted into the mask to prevent leakage of isoflurane. The whole anesthesia was monitored by a licensed veterinarian. After the rats woke up, the rats were put into individual cages for anesthesia and body temperature recovery. Eventually, the rats returned to the usual cage and access to standard food and water *Ad libitum*.

### 1.2.6 Conventional echocardiographic assessment

After Three weeks of the abdominal coarctation operation, all rats were anesthetized with 2.5% isoflurane with a 1L/min oxygen supply delivered through a mask. The echocardiography was carried out when the HR is stabilized. In this way, the mitral inflow pattern and HR were beyond the effect of environmental stimulation and anesthesia. Briefly, the rats were put on right and left lateral recumbency (41). The morphologic parameter including left ventricle end-diastolic diameter and left ventricle end-systolic diameter were sampled by the M-mode at the short axis view. Mitral inflow was sampled in the left apical 4-chamber view, and the mitral inflow velocity (E and A) and mitral inflow pattern were obtained. All measurements were taken from 5 times consecutive heart cycles and the average of the obtained parameters was used.

Left ventricle mass was calculated with the below formula:

$$LVM = 1.04 * ((\text{left ventricle end} - \text{diastolic diameter})^3 - (\text{left ventricle end} - \text{systolic diameter})^3)$$

### 1.2.7 Tissue Doppler imaging

Tissue Doppler imaging (TDI) was performed from the left apical 4-chamber view as shown in Figure 1-2. The LV septal and lateral wall movement were sampled by pulsed wave TDI echocardiography with a sample volume of 0.5 mm. The TDI velocity profile includes diastolic velocities (E' and A') at the point of attachment of the mitral valve to the septal and lateral walls of the LV were recorded.

E/E' was calculated by the below formula:

$$E/E' = \frac{\left( \frac{\text{E wave velocity}}{\text{E' posterior velocity}} + \frac{\text{E wave velocity}}{\text{E' anterior velocity}} \right)}{2}$$

LV end-diastolic pressure (LVEDP) and LV diastolic pressure at the onset of the a-wave (Pre-A LVDP) was calculated by the linear regression equation from invasive catheterization and E/E' (42).

$$\text{LVEDP} = 17.1 + 0.19 * E/e'$$

$$\text{Pre - A LVDP} = 6.97 + 0.3 * E/e'$$

### 1.2.8 Colour-M-mode-echocardiography for assessment of IVPG

Colour-M-mode-echocardiography (CMME) was performed from the left parasternal apical 4-chamber view under the left recumbence gesture. The sample volume was parallel to the mitral inflow in the apical view (Figure 1-3, A) using an ultrasound system (Hitachi Aloka Medical ProSound Premier 75CV, Japan) which supports the CMME (Figure 1-3, B) with a 12-MHz probe. Prior machine setting was done for the proper tracing of the CMME which includes sweep speed 300 mm/s, colour baseline shift to -64 to increase Nyquist limit.

All images were analyzed with the Euler equation using MATLAB (Figure 1-3, C, The MathWorks, Natick, MA) as previously described (Greenberg et al., 2001; Takahashi et al., 2019), and the IVPG was obtained. The total IVPG was divided into two segments based on the one-third segments of LV length: the smaller segment near the mitral valve is the basal IVPG, and the mid-to-apical IVPG segment is the other two-thirds near the apical IVPG (Figure 1-3. D). Basal IVPG was proved correlated with LA pressure and mid-to-apical IVPG represents active relaxation of the LV (31). Each view was captured three consecutive images for further analysis and the average was used as IVPG value.

### **1.2.9 Statistical analysis**

All data were measured at least three times and are expressed as mean  $\pm$  SD. GraphPad Prism 8 (GraphPad Software, La Jolla, CA) was used to analyze the data and plot the graphs. The group (Sham vs HTN-CM) and mitral inflow patterns (EA-fusion, EA-half-separation, EA-separation) were considered as two variables which used for comparison by two-way ANOVA, and Tukey's test was used for the post hoc test for the parametric study.  $P < 0.05$  was considered statistically significant. The Pearson correlation and multiple regression analysis were performed by SPSS (IBM, Armonk, New York) to analyze the relationship between cardiac parameters and novel echocardiography.

A prior conversion of the subjective variable including mitral inflow patterns into numeric variables was performed before conducting the correlation analysis. For instance, mitral inflow pattern is coded as 1= EA-separation, 2= EA-half-separation, 3= EA-fusion. Then the IVPG, E/E', E, and E' were taken as variables to perform correlation tests with HR and mitral inflow patterns.

## **1.3 Results**

### **1.3.1 Conventional echocardiography**

Conventional echocardiography parameters were displayed in Table 1-1 and 1-2. The HTN-CM group showed elevated blood pressure (90.81 vs 160.79,  $p<0.001$ ) and LVM compared with the Sham group (0.86 vs 0.64,  $p<0.001$ ), respectively. The combination of these measurements confirmed the existence of HTN-CM. Besides, no difference was detected in the ejection fraction, which indicates a stable systolic function in HTN-CM rats. As expected, HR and E in EA-fusion rats were significantly higher than EA-separation rats in both groups.

### **1.3.2 Tissue Doppler imaging**

In sham and HTN-CM rats, elevated myocardium movement and mitral inflow velocity indicate hyperdynamic states in EA-fusion pattern rats (Table 1-1). E/E' in the HTN-CM rats was higher than Sham rats in EA-fusion and EA-separation patterns and higher than 15, although not significant. The E/E' in HTN-CM group rats higher than 15 suggested diastolic dysfunctions although not significantly higher than Sham rats. E/E' was lower in EA-fusion rats compared with EA-half-separation and EA-separation groups, respectively in sham (13.21 vs 16.68,  $p<0.001$ ) and HTN-CM rats (14.47 vs 17.79,  $p<0.001$ ). This leads to the significantly lower LVEDP and Pre-A LVDP of EA-fusion rats in Sham and HTN-CM groups ( $p<0.001$  and  $p<0.001$ ).

### **1.3.3 IVPG measurements**

The IVPG data are summarized in Figure.1-4. In the sham group, the total IVPG, basal IVPG, and mid-to-apical IVPG were significantly higher in EA-fusion than in EA-separation rats (2.61, 1.60, 1.01 vs 2.26, 1.38, 0.88,  $p=0.000, 0.008, 0.015$ ), respectively. Also, EA-fusion rats were significantly higher than EA-half-separation in the sham group in terms of the total IVPG and mid-to-apical IVPG (2.61 and 1.01 in EA-fusion vs 2.27 and 0.86 in EA-half-separation,  $p=0.005$  and  $0.024$ ). Meanwhile, in HTN-CM rats (Figure. 1-3.D, E, F), only basal IVPG showed a significant difference between EA-fusion and EA-separation rats (1.68 vs 1.54,  $p=0.027$ ).

### **1.3.4 Pearson's Correlations test of the novel echocardiography**

Table 1-3 showed the correlation results between the E/E', IVPG, and other cardiac parameters. HR showed a significant positive correlation with IVPG, E, and E' average; meanwhile, HR revealed a significant negative correlation with E/E'. HR was significant weakly correlates with mid-to-apical IVPG, and HR significantly moderately correlates with Total, basal IVPG.

Because the mitral inflow pattern is transferred from string variables into numerical variables, the correlation ( $r$ ) is a relative value rather than an absolute value. In this regard, the mitral inflow pattern significantly weakly correlates with total and basal IVPG, while the mitral inflow pattern did not correlate with mid-to-apical IVPG. The mitral inflow patterns showed a significant moderate positive correlation with E, and E'; meanwhile, the E/E' showed a significant moderate positive correlation with the mitral inflow pattern. And the HR also correlates with the mitral inflow pattern.

## 1.4 Discussion

Elevated blood pressure supports hypertension, combine with the elevated LVM, HTN-CM is recognized in the HTN-CM group (43). However, in hypertension patients, the baseline resting HR is higher than 85 bpm, leading to a shrunk value of echocardiography because of the changed mitral inflow pattern (44, 45). In the current study, I choose the surgical hypertension model to mimic early-stage HTN-CM patients in this study (46). Instead of intentionally control the anaesthesia depth to achieve a certain HR, I performed echocardiography under the same isoflurane dose to make sure the influence of anesthesia was the same to every rat.

The purpose of the present study was to reveal whether IVPG and E/E' are affected by mitral inflow patterns or not. Our result showed, for the first time, that IVPG was weakly influenced by mitral inflow patterns, while mitral inflow patterns affect the E/E'.

The different mitral inflow patterns had different IVPG values as shown in Figure. 1-4. In EA-fusion rats, the pressure built up by accumulated pulmonary venous blood in the atrium combined with the left atrial contraction resulted in promoted LV inflow speed, volume, and LV myocardium movement (47). The total and basal IVPG elevation explained the promoted myocardium movement in the EA-fusion rats. The basal IVPG is well connected with LA pressure. Likewise, the elevated LA pressure and volume in EA-fusion rats led to promoted basal IVPG (31). In the present study, mid-to-apical IVPG was significantly increased in EA-fusion rats in the sham group. The development of compensated hypertrophy leads to the non-significant increased mid-to-apical IVPG in HTN-CM rats. Mitral inflow pattern is not correlated with mid-to-apical IVPG, because mid-to-apical IVPG illustrates the active relaxation which stays at the same level when the mitral inflow pattern changes.

E/E' was well correlated with Pre-A LVDP and LVEDP (48). The LVEDP is the same thing as Pre-A LVDP in EA-fusion rats because the E wave is merged with the A wave in EA-fusion patterns. However, based on the theoretical calculation, the LVEDP (19.61) was approximate twice the Pre-A LVDP (11.31) in EA-fusion rats, which showed the challenge of using E/E' to speculate LVEDP and Pre-A LVDP in EA-fusion rats.

The result of Pearson's correlation test indicates that the mitral inflow pattern significantly moderates correlates with HR. When the HR increases the mitral inflow changed from EA-separation to EA-fusion, and the Total IVPG, basal IVPG, E, and E' average also increases.

However, the E/E' is weakly negatively associated with HR and it is significant because the E' elevated more than E velocity. EA-fusion pattern owns the lowest preload among the 3 patterns because it owns only one inflow while the EA-separation pattern has two mitral inflow. Similarly, preload affects E' velocity more than E velocity (48), and I proved that the mitral inflow patterns correlate more with E' than E ( $r=0.443$  vs  $0.218$ , Table 1-2). Because E/E' was calculated by E velocity and E', the changed mitral inflow patterns lead to the uncertainty of E/E'. This explained why mitral inflow patterns affect E/E'.

## **1.5 Limitation**

In the present work, only female rats were included in this study. Although both genders develop hypertension, males have a higher incidence and severity of hypertension compared with peer females until they are sixty over. However, the physiological difference including growing speed in young rats may interfere homogeneous HTN-CM model.



## 1.6 Clinical implication

In clinical settings, physicians generally perform echocardiography when the HR is low and stable to avoid the EA wave fusion caused by high HR. However, in animal and human hypertension patients, the baseline resting HR is higher than 85 bpm, leading to a shrunk value of echocardiography because of the changed mitral inflow pattern.

Based on the result of this experiment, I found out that both E and E' in EA-fusion are higher than the EA-separation pattern. E/E' is lower in the EA fusion pattern. Thus, for the clinician, although performing echocardiography in low HR is still the best choice, intentionally controlling the HR during the IVPG test is not necessary, because id-to-apical IVPG was not impacted by the mitral inflow pattern.

## 1.7 Conclusion

Elevated HR leads to encroached diastasis, which eventually leads to an EA-fusion mitral inflow pattern. I proved that HR is associated with mitral inflow patterns. Both E and E' in EA-fusion are higher than the EA-separation pattern. The preload change has more impact on E' than E, which leads to decreased E/E' in EA-fusion. HR positively correlates with basal IVPG, E, and E', while mid-to-apical IVPG was independent of mitral inflow patterns. I conclude the principle of the IVPG test that intentionally controlling the HR to obtain IVPG is not necessary because the impact of HR on IVPG is weak. The result of this chapter established a solid foundation of evaluation of cardiac function noninvasively during the development of cardiac remodeling.

Table 1-1. Comparison of conventional echocardiographic parameters in Sham and HTN-CM groups regarding the pattern of the mitral inflow

Group	Sham group			HTN-CM group		
Patterns	EA-fusion	EA-half-sep. (n=7)	EA-sep.	EA-fusion	EA-half-sep.	EA-sep.
Parameters	(n=7)		(n=19)	(n=15)	(n=25)	(n=26)
LVM (g)	0.62±0.13 <sup>c</sup>	0.62±0.11 <sup>c</sup>	0.65±0.13 <sup>c</sup>	0.83±0.23 <sup>ab</sup>	0.86±0.31 <sup>a</sup>	0.87±0.35 <sup>a</sup>
EF (%)	75.13±5.12 <sup>a</sup>	71.93±6.8 <sup>a</sup>	70.37±10.63 <sup>a</sup>	70.21±9.68 <sup>a</sup>	70.9±8.33 <sup>a</sup>	65.33±6.14 <sup>a</sup>
E (m/S)	1.01±0.13 <sup>abc</sup>	0.96±0.11 <sup>bcd</sup>	0.90±0.10 <sup>d</sup>	1.06±0.13 <sup>a</sup>	1.02±0.16 <sup>ab</sup>	0.93±0.09 <sup>cd</sup>
A (m/S)	ND	ND	0.63±0.16	ND	ND	0.64±0.11
HR (bpm)	359.72±42.3 <sup>a</sup>	315.77±54.10 <sup>b</sup>	304.14±43.97 <sup>b</sup>	350.32±40.39 <sup>a</sup>	348.48±36.11 <sup>a</sup>	306.22±39.68 <sup>b</sup>
E/A ratio	ND	ND	1.57±0.09	ND	ND	1.49±0.04
E' (cm/S)	7.74±0.84 <sup>a</sup>	5.67±0.71 <sup>bc</sup>	5.51±0.81 <sup>c</sup>	7.59±1.13 <sup>a</sup>	6.22±1.03 <sup>b</sup>	5.40±0.76 <sup>c</sup>
E/E'	13.21±2.13 <sup>b</sup>	17.27±2.52 <sup>a</sup>	16.68±2.64 <sup>a</sup>	14.47±2.93 <sup>b</sup>	16.91±2.78 <sup>a</sup>	17.79±2.85 <sup>a</sup>
LVEDP (mmHg)	19.61±0.41 <sup>b</sup>	20.38±0.48 <sup>a</sup>	20.27±0.50 <sup>a</sup>	19.61±0.41 <sup>b</sup>	20.31±0.53 <sup>a</sup>	20.48±0.54 <sup>a</sup>
Pre-A LVDP (mmHg)	10.93±0.64 <sup>b</sup>	12.15±0.76 <sup>a</sup>	11.97±0.79 <sup>a</sup>	11.31±0.88 <sup>b</sup>	12.04±0.83 <sup>a</sup>	12.31±0.85 <sup>a</sup>
SAP (mmHg)	95.05±9.02 <sup>c</sup>	89.28±11.4 <sup>c</sup>	89.79±13.9 <sup>c</sup>	169.26±18.69 <sup>ab</sup>	166.38±13.42 <sup>a</sup>	150.76±19.64 <sup>b</sup>

Echocardiographic measurements in sham and hypertensive cardiomyopathy (HTN-CM) rats after 3 weeks. Each group was classified according to the mitral inflow pattern. The group (Sham vs HTN-CM) and mitral inflow patterns (EA-fusion, EA-half-separation, EA-separation) were considered as two variables which used for comparison by two-way ANOVA, Tukey test was used for post hoc comparison. The letters are fitted for comparing means between groups and different letters in the same row indicates significant difference ( $p < 0.05$ ). sep., separation; LVM, left ventricle mass; E, the velocity of early mitral inflow; Peak A, the velocity of late mitral inflow; HR, heart rate; E', Peak velocity of early diastolic mitral annular motion as determined by pulsed-wave Doppler; E/E', Ratio of E to E'; LVEDP, left ventricle end-diastolic pressure; Pre-A LVDP, left ventricle diastolic pressure at the onset of the A-wave; SAP, systolic arterial pressure. ND, not detected.

Table 1-2. Morphologic echocardiography

	Sham rats			HFpEF rats		
patterns	EA fusion(n=21)	EA half separation(n=20)	EA separation(n=57)	EA fusion(n=32)	EA half separation(n=54)	EA separation(n=57)
IVSd (mm)	1.19±0.17 <sup>**!!</sup>	1.21±0.12 <sup>**!!</sup>	1.18±0.16 <sup>**!!</sup>	1.57±0.25 <sup>##‡‡</sup>	1.67±0.35 <sup>##‡‡</sup>	1.68±0.38 <sup>##‡‡</sup>
LVIDd (mm)	7.13±0.61	7.23±0.82	7.49±0.65 <sup>*!</sup>	6.97±0.64 <sup>‡</sup>	7.13±0.64	7.06±0.91 <sup>‡</sup>
LVPWd (mm)	1.52±0.33	1.47±0.3 <sup>!</sup>	1.48±0.31 <sup>**!!</sup>	1.9±0.38 <sup>‡‡</sup>	1.83±0.42 <sup>‡‡</sup>	1.93±0.93 <sup>‡‡</sup>
IVSs (mm)	2.12±0.35 <sup>!!</sup>	1.93±0.37 <sup>*!!</sup>	1.91±0.31 <sup>*!!</sup>	2.36±0.42 <sup>‡‡</sup>	2.51±0.43 <sup>##‡‡</sup>	2.46±0.39 <sup>##‡‡</sup>
LVIDs (mm)	3.89±0.42 <sup>‡</sup>	4.14±0.53	4.37±0.69 <sup>#!</sup>	4.09±0.75	4.15±0.66	4±0.52 <sup>‡</sup>
LVPWs (mm)	2.46±0.44	2.37±0.35 <sup>‡</sup>	2.23±0.34 <sup>‡‡!!</sup>	2.73±0.34 <sup>‡‡</sup>	2.67±0.42 <sup>‡‡</sup>	2.66±0.44 <sup>‡‡</sup>
a' septum	ND	5.35±0.66	5.78±1.09	ND	6.24±1.05	5.64±0.79
a' free wall	ND	6.38±1.11	6.24±1.18	ND	6.98±1.23 <sup>!</sup>	6.28±1.28
a' average	ND	5.83±0.5	6.08±0.94	ND	6.55±1 <sup>!!</sup>	5.97±0.87
DAP, mmHg	57.94±9.06 <sup>‡***!!</sup>	55.27±4.34 <sup>**!!</sup>	51.31±8.77 <sup>**!!</sup>	89.43±6.97 <sup>####!!</sup>	86.22±8.26 <sup>####!!</sup>	75.47±7.98 <sup>####*</sup>
MAP, mmHg	71±2.11 <sup>‡***!!</sup>	67.99±1.67 <sup>***!!</sup>	62.85±3.45 <sup>####!!</sup>	127.83±18.8 <sup>####!!</sup>	113.43±9.12 <sup>####***!!</sup>	102.28±9.57 <sup>####***</sup>

Echocardiographic measurements according to the mitral inflow pattern in sham and HFpEF rats after 3 weeks of operation using one-way ANOVA. # indicates significantly different with EA fusion Sham rats, p<0.05, and ## indicate p<0.01; ‡ indicates significantly different with EA separation Sham rats, p<0.05, and ‡‡ indicate p<0.01; \* indicates significantly different with EA fusion HFpEF rats, p<0.05, and \*\* indicate p<0.01; ! indicates significantly different with EA separation rats, p<0.05, and !! indicate p<0.01. ND, not detected.

IVSd, interventricular septum diastolic diameter; LVIDd, left ventricular internal diastolic diameter; LVPWd, left ventricular posterior wall diastolic diameter; IVSs, interventricular septum systolic diameter; LVIDs, left ventricular internal systolic diameter; LVPWs, left ventricular posterior wall systolic diameter; EF, ejection fraction.; DAP, diastolic atrial pressure; MAP, mean atrial pressure.

Table 1-3. Pearson Correlations test of the echocardiography

Variables	HR		Mitral inflow pattern	
	r	p	r	p
Total IVPG	0.412**	0.000	0.265**	0.000
Basal IVPG	0.358**	0.000	0.270**	0.000
Mid-to-apical IVPG	0.188**	0.003	0.070	0.281
E/E'	-0.291**	0.000	-0.381**	0.000
E	0.218**	0.000	0.389**	0.000
E'	0.443**	0.000	0.665**	0.000
Mitral inflow pattern	0.434**	0.000	ND	ND

The relationship between E/E' and IVPG data and mitral inflow pattern as well as groups. Total IVPG, the mix of basal and mid-to-apical intraventricular pressure gradients; basal IVPG, the basal intraventricular pressure gradients; mid-to-apical IVPG, the mid plus apical intraventricular pressure gradients; HR, heart rate; E/e', E to mitral annulus velocity ratio; E, the velocity of early mitral inflow; E' average, average early diastolic mitral annulus velocity. \* indicates the  $p < 0.05$ , and \*\* indicates  $p < 0.01$ . ND, not detected.

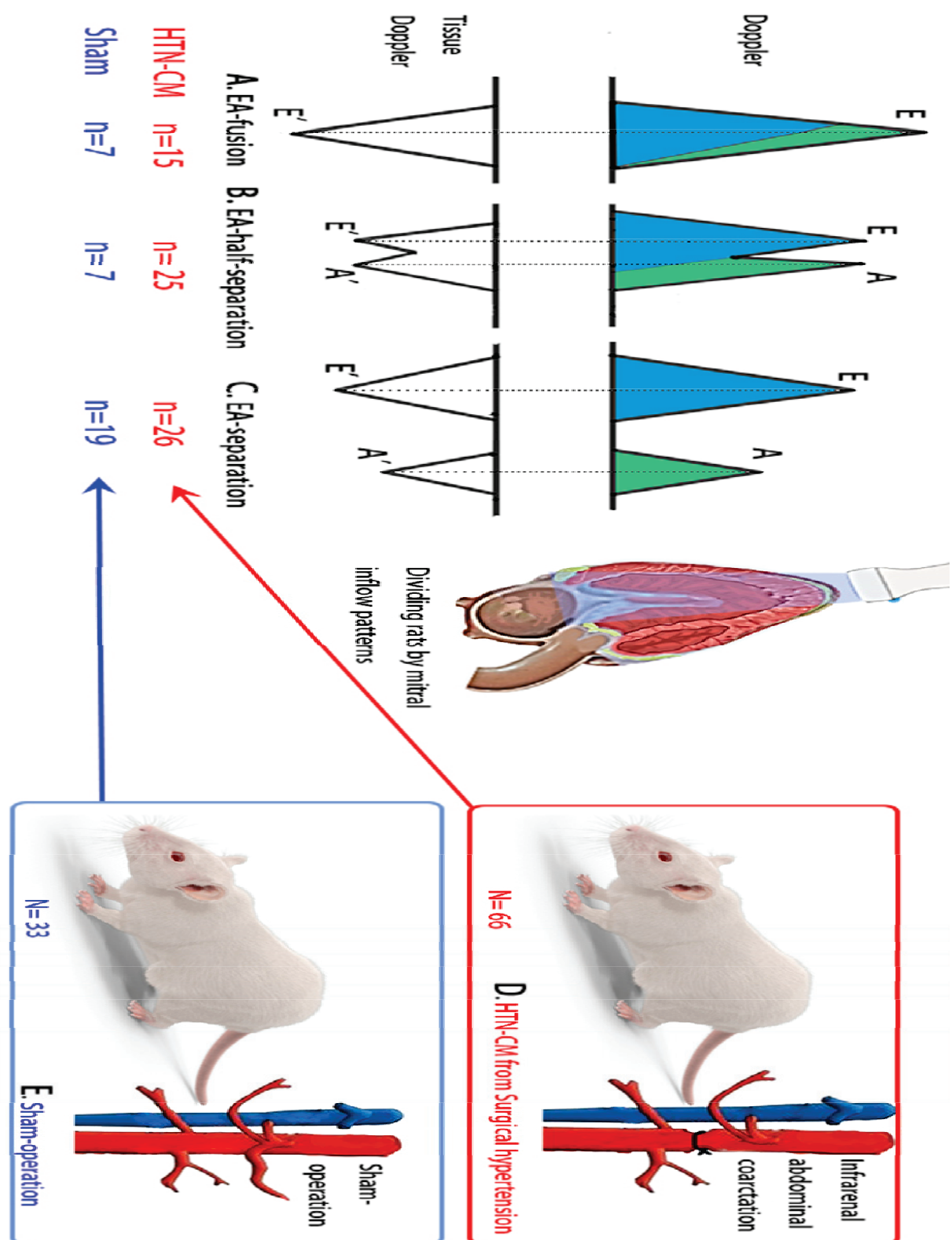


Figure. 1-1. Experiment design and mitral inflow patterns: The blue colour in the Doppler image indicates the volume of early diastole and the green colour represents the volume of atrial contraction A: EA-fusion pattern, indicating mixed early diastole and atrial contraction, B: EA-half-separation, C: EA-separation, D: HTN-CM from abdominal aorta coarctation, E: Sham-operation

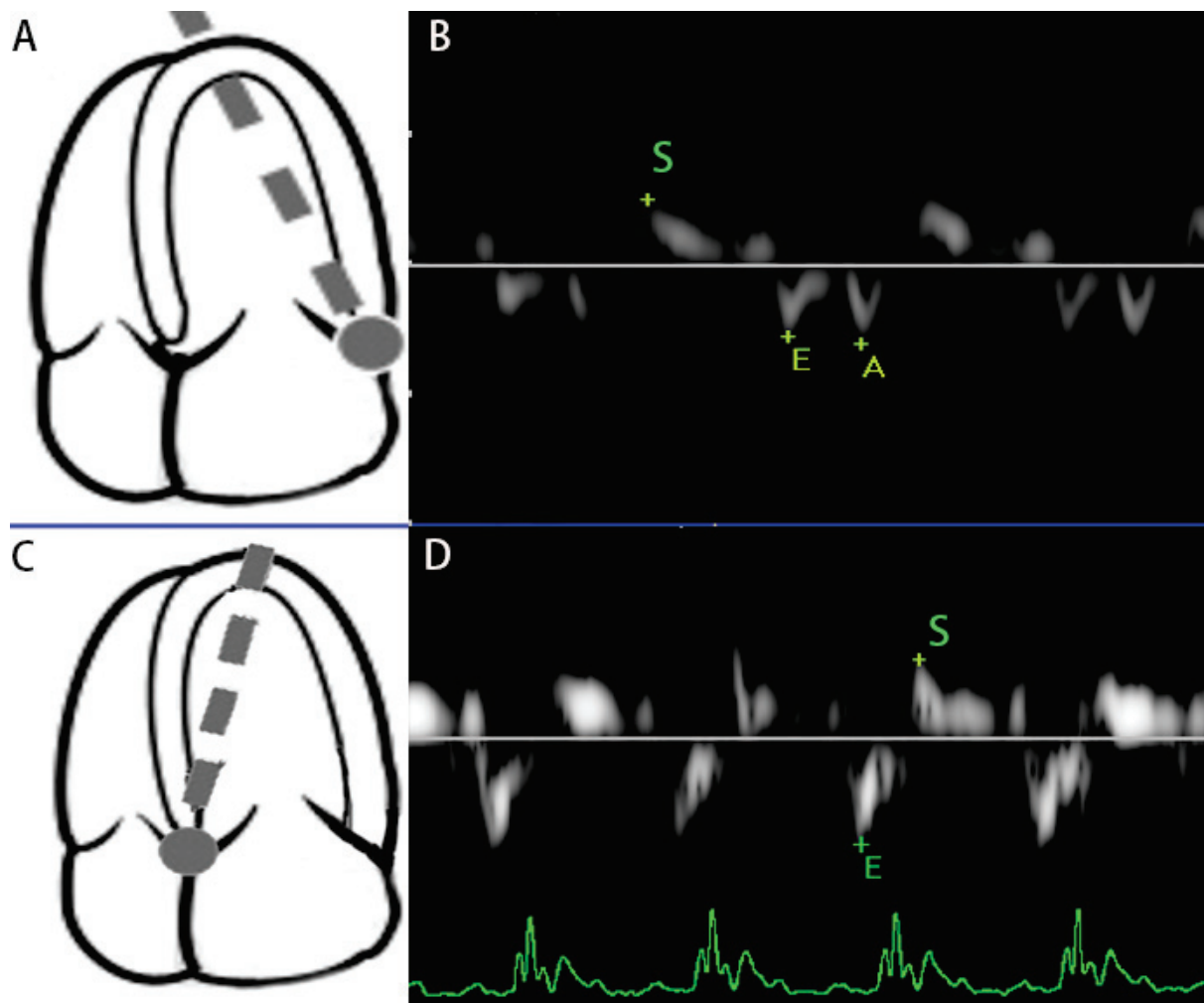


Figure 1-2. Tissue Doppler imaging was sampled from the free wall(A) and septum(C) mitral annular movement. The B illustrates the 3 basic waveforms of tissue Doppler interrogation: S' (systolic myocardial motion), E (early diastolic motion), and A (atrial contraction). The D section illustrates sometimes, E and A waves mixed, indicating the early diastole and atrial contraction were merged.



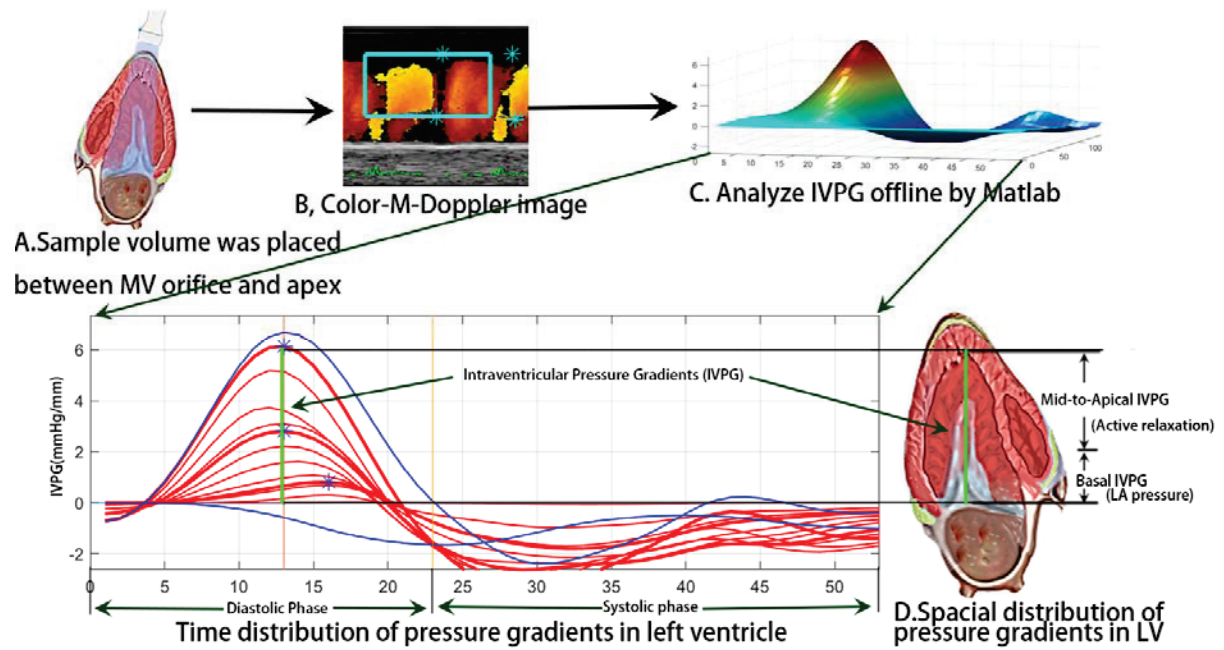


Figure. 1-3. Schematic illustration of IVPG measurement through image analysis of photos obtained from CMME in left apical four-chamber view using Matlab software.

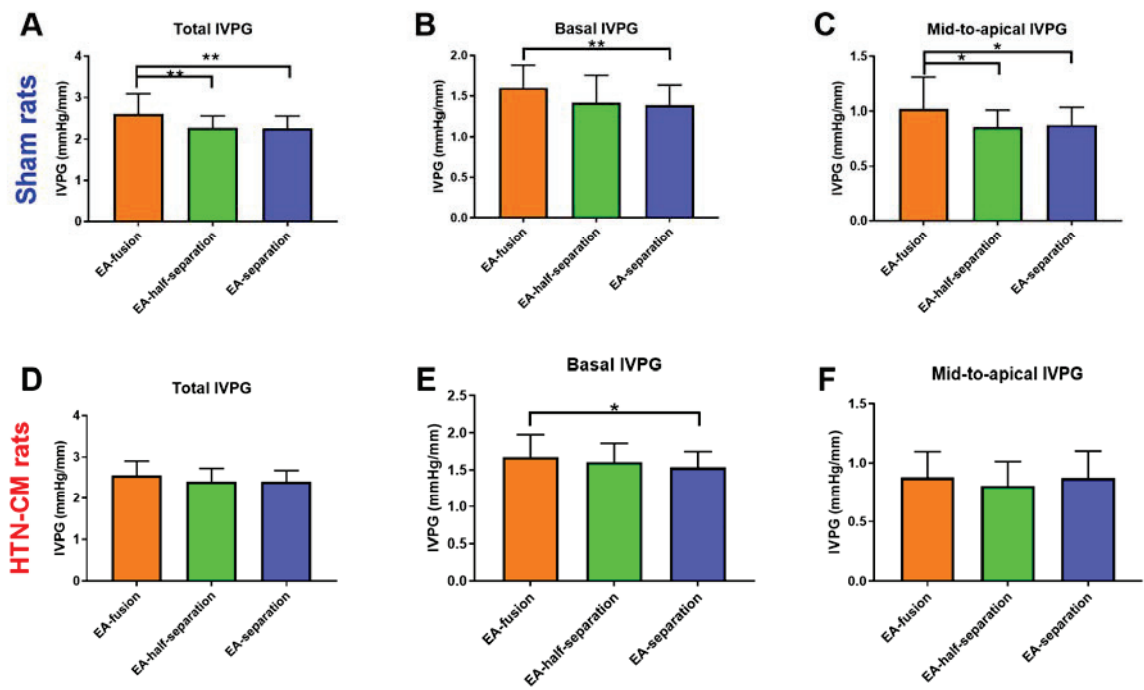


Figure. 1-4. Comparison of IVPG data according to the mitral inflow pattern (EA-fusion, EA-half-separation, and EA-separation) in Sham (A, B, C) and HTN-CM (D, E, F) groups.

## **Chapter 2**

### **Investigation of the cardiac function in pressure-overload model**

## 2.1 Introduction

From chapter 1, I obtained the principle of the IVPG test to evaluate cardiac function noninvasively, that intentionally controlling the HR during the IVPG test is not necessary. To achieve further pathophysiology of CVDs, this chapter describes a quantitative study of the exploring pathophysiology of pressure overload. Pressure overload is the most common form of cardiac stress that may induce ventricular remodeling. Pressure overload initiates a series of events including a change of the chamber architecture, and eventually congestive heart failure(CHF) (49). The most common CVDs entities that exert pressure overload are hypertension. Hypertension, as known as high blood pressure, is a long-term medical condition associated with considerable morbidity and mortality(1).

Hypertensive cardiomyopathy (HTN-CM), a structural cardiac disorder, is characterized as concentric left ventricular hypertrophy (LVH) associated with systolic or diastolic function coexisted with systemic hypertension (50). The excess pressure from hypertension forces the heart to progressively remodeling against the elevated artery resistance. Although LVH can happen earlier than the development of hypertension, the progression in hypertensive cardiomyopathy from simple LVH to congestive heart failure (51).

Chronic pressure overload causes progressive cardiac remodeling, resulting in HTN-CM, and subsequently leads to diastolic dysfunction and congestive heart failure. The HTN-CM is thought to play a compensatory role in enhancing cardiac performance to compensate for pressure overload, but this maladaptive response ultimately hurts patients(52). Beta-adrenoceptor is activated during this process, elevating the levels of cAMP, PKA, and  $\text{Ca}^{2+}$ , leading to an increase in the heart rate and myocardial contractility. Thus, beta-blocker like Carvedilol and sotalol has been used in the treatment of HTN-CM. Beta-blockers are widely prescribed to heart failure patients despite a lack of compelling indication for use, and the

association of beta-blocker use with heart failure hospitalization grows the need for another medication to overcome the disadvantages of beta-blocker for future replacement (53, 54).

Abdominal aortic coarctation elevates the cardiac afterload, then the compensatory LVH developed, gradually lead to pathological hypertrophy characterized by myocardial fibrosis (55). The abdominal aortic coarctation model was mainly used to study cardiovascular damage in hypertension, because the blood pressure is gradually elevated, and the fluctuation was also low (56).

Salvianolic acid B (Sal B) is the main constituent of *Salvia* phenolic acids derived from the dried root and rhizome of *Salvia miltiorrhiza* Bge (Labiatae) which has been used widely in Asian countries particularly in China for cardiovascular disorder. Sal B was reported to protect myocardial cells from apoptosis *in vivo* and *vitro* (57). Cardiac fibroblasts play a key role in cardiac function, and Sal B downregulates the cardiac fibroblast, which is important in cardiac remodelling (58). The preclinical studies revealed that Sal-B could alleviate ischemia-induced myocardial injury and modulate angiogenesis *in vivo* (59). Therefore, Sal-B may be a hopeful therapy to treat HTN-CM from pressure overload. But the hemodynamic and morphology effect of Sal B in the pathologic model is still unknown. In short, Sal B can prevent cell proliferation, and hyperplasia, which indicates it may have a treatment effect on LV hypertrophy. To evaluate Sal-B as a putative medicine for the treatment of HTN-CM, its cardiovascular effects in this context will be monitored.

In diastole, the force sucking blood from the LA to the LV is correlated with *Tau*, the time constant of LV pressure decay. *Tau* is known as the gold standard for the measurement of diastolic function and it is a source of the intraventricular pressure gradients (IVPG). In clinical settings, non-invasive measurement of IVPG using analysis of colour M-mode images provides a practical means to evaluate diastolic function (20, 60, 61).

The cardiac diastolic function relies on active myocardial relaxation and the passive property of the ventricle wall. Since IVPG reveals active relaxation status and LA pressure(31, 62), investigating the IVPG status during the pathogenesis of HTN-CM could yield new insights into the mechanisms of diastolic dysfunction. Even though the difference between heart failure patients and healthy humans is well described, the chronological order during the development of heart failure is still unknown(63, 64). Identifying the chronological order during the development of diastolic dysfunction would contribute to a more accurate diagnosis, and it will elucidate the relationship between hemodynamic status and morphological changes in cardiac remodeling.

Although therapeutic modalities for HTN-CM have been thoroughly investigated, the therapeutic threshold of pharmacological interventions may vary between patients. Precise diastolic monitoring after therapeutic interventions using technologies such as IVPG could allow evaluation of treatment efficacy in clinical settings (65), thereby allowing physicians to tailor treatments to each patient.

My aim in this chapter was to evaluate the cardiac function change during the development of pressure overload and to evaluate the treatment effect of Salvianolic acid B.

## **2.3 Materials and methods**

### **2.3.1 Animal**

Eighty female Sprague Dawley rats two months of age ranging from 230 to 260 g were supplied water and food ad libitum and housed at 22°C on a 12-hour light/dark cycle. All procedures and protocols used in this experiment were performed and approved under the

standard guidelines described in “Guide for the Care and Use of Laboratory Animal” of Tokyo University of Agriculture and Technology. The study was approved by the Animal Care and Use Committee of the Tokyo University of Agriculture and Technology (30-56).

### **2.3.2 Induction of hypertensive cardiomyopathy**

Abdominal aorta coarctation surgery of the abdominal aorta was performed in 68 rats as described previously. Briefly, female Sprague Dawley rats were anesthetized with 50 mg/kg intraperitoneal Pentobarbital sodium. Rats were placed supine under an operating microscope (Leica M60, Wetzlar, Germany). The abdominal aorta was exposed using a cotton swab and sutured together with a blunt 22-gauge needle with 3-0 silk. The needle was then withdrawn to create appropriate stenosis in the abdominal aorta. Eight rats were excluded due to death within three weeks after the operation, and twelve rats were excluded due to lack of a systolic abdominal aorta stenosis peak speed lower than 2 m/s.

### **2.3.3 Research design**

The spotlight of this research is the abdominal coarctation operation was more homogeneous compare with the other research. In this study, I performed a coarctation operation in 56 rats and then take the abdominal ultrasound of aorta blood speed 3 weeks after the operation. 20 rats were excluded from the original study because of death within three weeks (8 rats) and systolic abdominal aorta stenosis (peak speed lower than 2 m/s, 12 rats). And the 36-success produced abdominal coarctation were randomly divide into HTN-CM, Carvedilol, and Salvianolic acid B group.

Three weeks postoperatively, the 36 successfully operated rats were randomly divided into three equal subgroups: HTN-CM group, Sal-B group, and Carvedilol group (n = 12) as shown in Figure. 2-1. Another 12 Sham-operated rats were used as a Sham group. The treatment protocol includes administration of Sal-B (5 mg/kg/day, I.P, Danshen DuofensuanYan 100mg, GreenValley Inc, Shanghai, China), Carvedilol (2 mg/kg/day, P.O, Artist Tablets 2.5mg, Daiichi-Sankyo, Tokyo, Japan), and normal saline to the HTN-CM and Sham groups (Figure. 2-1). After confirming the existence of HTN-CM by elevated relative wall thickness (RWT), blood pressure, and left ventricular mass (LVM) three weeks postoperative, the treatments were administered once daily till the end of the six weeks to allow longitudinal evaluation.

### **2.3.4 Echocardiographic measurements**

Sham and HTN-CM groups were sampled at 0, 0.5, 1, 2, 3, 4.5, and 6 weeks after the operation, while the two treatment groups Sal-B and Carvedilol were examined at 4.5 and 6 weeks after operation as shown in Figure 2-1. The time frame of measurement was decided by the development of HTN-CM and the effect of treatment as modified from previous reports (66).

Rats were positioned under an inspiratory anesthesia mask administering 2.5% isoflurane at 1L/min oxygen. Noninvasive systemic vascular resistance measurements were obtained by abdominal aortic ultrasound in the prone decubitus position under anesthesia (ProSound F75 Premier CV, Hitachi Healthcare System Inc, Tokyo, Japan). A 1 mm sample volume was placed at the abdominal aorta stenosis to measure the degree of stenosis using a 5-15 MHz continuous-wave transducer as shown in Figure 2-2.

Conventional echocardiography was also performed. Morphology data were sampled by M-mode tracing on the right parasternal short-axis image at the papillary muscle level of the



LV. The following parameters were obtained: LV diastolic (d) and systolic (s) diameters (LVIDd and LVIDs, respectively), LV diastolic and systolic posterior wall thickness (LVPWd and LVPWs, respectively), and septal diastolic and systolic wall thickness (IVSd and IVSs).

LVM and RWT were calculated with the below formulas:

$$LVM = 1.04 * ((\text{left ventricle end} - \text{diastolic diameter})^3 - (\text{left ventricle end} - \text{systolic diameter})^3)$$

$$RWT = \frac{IVSd + LVPWd}{LVIDd}$$

### 2.3.5 Tissue Doppler imaging

A left parasternal apical four-chamber view was obtained for mitral valve (MV) inflow assessment and tissue Doppler imaging (TDI). The early diastolic (E) and atrial systolic (A) wave peak velocities of the mitral inflow were measured using pulsed-wave Doppler echocardiography. The early (E') and late (A') diastolic velocities of the posterior and anterior myocardial wall at the point of attachment to the MV were measured by pulsed-TDI. The TDI was calculated using the below formula:

$$E/E' = \left( \frac{E \text{ wave velocity}}{E' \text{ posterior velocity}} + \frac{E \text{ wave velocity}}{E' \text{ anterior velocity}} \right) / 2$$

The LV function was evaluated by fractional shortening (FS) and the E/A velocity ratio of the mitral inflow. Every measurement was repeated five times at each experimental time interval, and the average value was used for data analysis.

### **2.3.6 Colour M-mode echocardiography derived intraventricular pressure gradients**

Colour M-mode echocardiography with simultaneous electrocardiography (ECG) was recorded with the cursor parallel to the mitral inflow in the apical four-chamber view under the left recumbence gesture, and the rat's limbs were tightened with micropore paper tape. The sampling was only processed when the respiratory rate of rats was stable (25-35 cycles per minute). Heart rate was not controlled during the sampling to avoid interference between anesthesia and circulation.

Colour M-mode images were analyzed with the Euler equation by Matlab (The MathWorks, Natick, MA) to obtain the intraventricular pressure difference. IVPG was calculated using the below formula:

$$\text{IVPG} = \frac{\text{intraventricular pressure difference}}{\text{LV length at the end of the diastole phase}}$$

The total IVPG was divided into two segments based on one-third segments of LV length, where the smaller segment near the mitral valve was basal IVPG, and the mid-to-apical IVPG segment was the other two-thirds near the apex as shown in Figure. 2-3. Two independent observers from Juntendo University analyzed the same images, and one blinded observer repeated the analysis on a different day. All data were measured at least five times at each interval time and the average data were reported.

### **2.3.6 Blood pressure**

Blood pressure was monitored in caged rats by the oscillometric method from the tail (BP monitor for rats, Muromachi, Japan). At least 5 consecutive measurements at each time interval

were taken and the average of the systolic, diastolic and mean arterial blood pressure has been reported.

### **2.3.7 Statistical analysis**

All data measurements were tested by the Sidak test in the Two-way factorial ANOVA while the two variables (group and time) were considered. The Turkey test was used in the treatment reviewing two-way ANOVA multiple comparison test. Results are expressed as mean $\pm$ SD and P-value <0.05 was considered statistically significant. The data were analyzed and graphed using GraphPad Prism 7 (GraphPad Software, San Diego, CA).

## **2.4 Results**

### **2.4.1 Conventional echocardiography measurements and blood pressure**

The conventional echocardiographic data and the blood pressure throughout the experimental intervals are summarized (Table 2-1&2-2, Figure. 2-4&2-5). There was no significant difference in the HR and TDI among all 4 groups at 4.5 and 6 weeks (Figure. 2-4.A&C). HTN-CM was confirmed by the elevated LVM after 4.5 weeks (Figure. 2-5, B and Table 1), and HTN-CM was concentric because the RWT is higher than 0.42. The LVM of the HTN-CM group was higher than the Sham group at 4.5 weeks (1.52.vs 1.20, P=0.026) and 6 weeks (1.58 vs 1.16, P=0.002), respectively. Also, the LVM in the Carvedilol group was higher than the Sham groups at 6 weeks (1.47 vs 1.16, P=0.030), meanwhile, the LVM in the Sal-B group did not show a significant difference with the Sham group (Figure. 2-5.B).

The Systolic artery pressure in the HTN-CM group from 2 to 6 weeks was significantly higher than that of the Sham group (Figure. 2-5.D). Besides, the systolic artery pressure in the

Sham group was significantly lower than other groups at 4.5 weeks and did not show a significant difference with the Sal-B group at 6 weeks (Figure. 2-5.D). This indicates that the blood pressure-lowering effect of Sal-B is less than Carvedilol. Other conventional echocardiographic parameters are listed in Table 2-1& 2-2.

#### **2.4.2 IVPG measurements**

IVPG characteristics in the Sham group and HTN-CM group at different time points are shown in Figure. 2-6 (A, B, C). The total IVPG was significantly different among different time points and groups ( $P<0.001$ ). In the HTN-CM group, the total IVPG was increased at approximately 0.5 weeks and then decreased until two postoperative weeks in aortic coarctation groups, followed by a significant increase at 4.5 and 6 weeks compared with the Sham group.

Also, the basal IVPG of the HTN-CM group was significantly higher than the Sham group at 3 and 6 weeks. Meanwhile, no significant difference was detected in mid-to-apical IVPG between Sham and HTN-CM groups.

The total IVPG was significantly different among the four groups at 4.5 weeks ( $P<0.0001$ , Figure. 2-5, D). But mid-to-apical IVPG of the non-treating group was higher than the Sal-B group at 4.5 weeks, indicating that the active relaxation of the HTN-CM group was higher than the Sal-B group, which may be connected with the lower LVM in the Sal-B group.

The total IVPG (2.646) and basal IVPG (1.747) in the HTN-CM group were higher than that of the Sham group (2.182 and 1.354) at 6 weeks ( $P<0.001$ ,  $P<0.001$ , respectively).

Carvedilol showed a therapeutic effect by significantly lower total IVPG (2.395) and basal

IVPG (1.512) value at 6 weeks compared with the HTN-CM group ( $P=0.001$  and  $0.026$ , respectively).

Similar to Carvedilol, the Sal-B also exhibited a treatment effect by decreasing the total IVPG (2.395) and basal IVPG (1.521) value at 6 weeks compared with the HTN-CM group ( $P=0.0296$  and  $0.0469$ , respectively). As expected, no difference was detected in the mid-to-apical IVPG among groups at 6 weeks ( $P=0.1034$ ) as shown in Figure. 2-5 (D, E, F).

## 2.5 Discussion

From the study in chapter 1, I obtained the setting of IVPG in a rodent model. Thus, in this experiment, the heart rate was not intentionally controlled. Once the rats have stable respiration and stay in the proper anesthesia stage, the IVPG test was performed.

The clinical application of IVPG requires an explicit understanding of IVPG spatial distribution. Iwano *et al.* demonstrated that basal IVPG correlated with LA pressure(67), and mid-to-apical IVPG has been demonstrated to represent active relaxation during diastole(62). Thus, IVPG provides a tool for evaluating cardiac function. which can be used clinically to distinguish among different pathological features of diastolic dysfunction.

Abdominal aorta coarctation surgery dramatically increases the afterload and leads to HTN-CM(68), which was consistent with the results in the present study. RWT higher than 0.42 and elevated LVM in the HTN-CM group at 4.5 and 6 weeks indicates that the heart eventually developed concentric HTN-CM(69). Besides, hypertrophy in the two treatment groups was not as severe as the HTN-CM group as shown in Table 2-2.

The increased total IVPG at 0.5 weeks postoperative in the HTN-CM group was caused by the surgery, as the Sham group had a similar fluctuation. The increased total IVPG was

primarily contributed by elevated basal IVPG, although no difference in the basal IVPG was observed. Total IVPG was significantly higher in the HTN-CM group than in the Sham group from 4.5 to 6 weeks. This has been attributed to higher basal IVPG, which reflects the increased LA pressure at this time. Also, the elevated LA pressure and Left ventricle end-diastolic pressure (LVEDP) was reported in this model (70).

The mid-to-apical IVPG in the HTN-CM group stays at the same level as observed in the Sham group all over the study period. This finding indicates that the active myocardial relaxation and the passive property of the ventricular wall are not dramatically changed at the early stage of compensated HTN-CM(71).

Different from our primary hypothesis, severe diastolic dysfunction, decreased myocardium movement, and reduced mid-to-apical IVPG was not evidenced in the present study. Mild Diastolic dysfunction was observed at 2 weeks in elevated basal IVPG, but not significant. Besides, the systolic artery pressure in the HTN-CM group was significantly higher than in the Sham groups at 2 weeks. In contrast, the myocardial hypertrophy did not show up until 3 weeks as indicated by increased RWT. These results revealed that the hemodynamic changes precede the HTN-CM-related morphological changes in the current study (72).

Generally, the chronological order of the IVPG is explained as elevated basal IVPG and maintained mid-to-apical one in the early stages of HTN-CM, which implies elevated LA pressure and maintained active relaxation. It was speculated that the basal and mid-to-apical IVPG may decrease in the late stage of HTN-CM, since the heart may lose its ability to maintain the high LA pressure and active relaxation and compensated by the fibrosis and scarred myocardium in the late stage of HTN-CM (73). This requires further research of IVPG changes in the late-stage of HTN-CM.

LA pressure reflects LA function, but it was difficult to measure in rats directly by catheterization. This makes the indirect measurement of LA pressure by echocardiography the only practical method to estimate the LA function. In this regard, TDI, a cardiac performance assessment combined with both hemodynamic and myocardium movement, was considered a non-invasive technology in evaluating LA function. However, the sensitivity of TDI remains questionable recently, because the longitudinal regional strain is heterogeneous between humans and rats (74). Moreover, the myocardium movement in rats is different from humans for their higher heart rate and smaller heart size. This explains why the TDI shows no difference between the 4 groups at 4.5 and 6 weeks, while IVPG indicates the elevated LA pressure.

Although LA pressure was elevated during the development of HTN-CM, the elevation was not dramatic enough to be recognized by TDI. A significant increase in basal IVPG was observed that confirm elevated LA pressure, while the TDI fluctuated and did not change along with the experiment. Therefore, IVPG can be more promising in cardiac function evaluation than TDI as it avoids the species difference in myocardium movement (75).

Beta-blockers are the first-line medicine in treating HTN-CM by relieving the stress of the myocardium, which is achieved by slowing the heart rate and blood pressure as shown in Figure. 2-4. The elevated blood pressure in the Sal-B group at 6 weeks indicates that the treatment mechanism was different from Carvedilol.

Prescribing beta-blockers has been proved associated with higher mortality and higher brain natriuretic peptide (BNP) levels in heart failure patients compared with patients not receiving beta-blockers (76, 77). Beta-blockers own the demerits of tolerability and physicians have to follow up because beta-blockers need to titrate in clinical practice (78).

The therapeutic effects of Carvedilol and Sal-B seem difficult to evaluate from conventional parameters. In our model, many echocardiographic parameters did not change between groups. Nevertheless, the new parameter, IVPG, seems useful to evaluate the effect of the used drugs. Total IVPG was increased by basal IVPG elevation, which indicated that the treatments effectively reduce the LA pressure in compensatory hypertrophy. In the present study, Sal-B and Carvedilol did not reverse the cardiac function and HTN-CM into the intact level, but to gain more benefits, further studies are necessary to evaluate the response of IVPG and HTN-CM to the different dosage of Sal-B.

Carvedilol confers cardiac protection by blocking beta-1, 2, and alpha-1 adrenergic receptors, which reduce the IVPG in physiological heart remodeling (79). A similar effect was observed in the present study in the Sal-B group (Figure. 2-5). This could be explained by improving cardiac contractibility, attenuating hyper contraction, and reducing LVEDP after Sal-B administration(80). Pressure overload activates the metabolism of ERK (extracellular signal-regulated kinase), which promotes the expression of Gata4 and result in heart failure. Besides, Sal-B has been proven to decrease myocardial fibrosis and hypertrophy *in vivo* and *in vitro* by low down the level of ERK and Gata4 (70, 81), which might also be the therapeutic mechanism in Sal-B together with the beta-blocker effect (82-84). Although no evidence has suggested that Sal-B blocks beta-adrenoceptors directly, Lu et al. demonstrated that Sal-B had similar effects to a beta-blocker in decreasing  $Ca^{2+}$  and cAMP and inhibiting PKA activation (59). Scientists also proved that Sal-B owns the cardioprotective effect by inhibiting Gata4 gene expression, which controls the expression of atrial natriuretic peptide and BNP (73, 85).

Therefore, although the cardioprotective effects of Sal-B and Carvedilol did not differ significantly in our model, Sal-B may have therapeutic advantages over Carvedilol, as part of its effects is similar to beta-blocker and the other part is related to ERK/Gata4 to alleviate the



HTN-CM as shown in Figure. 2-6 (73, 86). Salvia Miltiorrhiza Depside Salt for infusion, which contains 60% of Sal-B, is well-tolerable and has fewer side effects than beta-blocker (87, 88).

Furthermore, beta-blockers are not recommended in hypertrophic obstructive cardiomyopathy (HOCM) by guidelines, and the refractory was reported in beta-blocker treatment (87, 89). Consequently, Sal-B might have potential therapeutic effects to treat HOCM because of low side effects and non-blood pressure-lowering effect (88), however, further study is needed in this regard.

As observed in the present chapter, the IVPG status has been evaluated in aortic coarctation-induced HTN-CM in the rat model with and without therapeutic interventions. First, the clinical meaning of IVPG spatial distribution was discussed. Second, the chronological order of IVPG during the development of HTN-CM was evaluated. Third, the hemodynamic effects of Sal-B and Carvedilol *in vivo* were described.

## 2.6 Limitation

**The invasive hemodynamics of hypertension rats is not measured because the unrepeatable of rat hemodynamic monitoring. The systemic vascular resistance increase only once and the operated rats' cardiac function would adjust to the pressure overload produced by binding rather than progressive increasing to heart failure.**

## 2.7 Conclusion

Based on the pathophysiology of cardiac remodeling, IVPG changes precede morphological disruption during the development of LVH, which indicates that the pressure

gradients change is more sensitive than morphological change during the development of cardiac remodeling. Sal-B and Carvedilol promote cardiac function by preventing the progressive elevation of basal IVPG in the LVH model. Sal-B could be a potential therapy for LVH, as its efficacy for treatment promotes cardiac function without lowering the blood pressure, which is different from Carvedilol.

Table 2-1. Longitudinal echocardiographic examination of the sham and HTN-CM groups throughout the entire experimental time-intervals

	Sham							HTN-CM						
Time/ week	0	0.5	1	2	3	4.5	6	0	0.5	1	2	3	4.5	6
IVSd (mm)	1.1±0.13	1.12±0.1	1.22±0.13	1.19±0.07	1.33±0.2	1.19±0.16	1.14±0.23	1.15±0.14	1.22±0.12*	1.20±0.08	1.19±0.11**	1.54±0.15**	1.68±0.28	1.73±0.34**
LVIDd (mm)	6.91±0.47	6.86±0.72	6.85±0.41	6.86±0.55	6.95±0.51	6.91±0.68	6.92±0.61	6.92±0.43	7.01±0.38	7.03±0.34	6.99±0.63	7.08±0.53	7.12±0.53	7.12±0.56
LVPWd (mm)	1.5±0.25	1.43±0.25	1.47±0.25	1.47±0.26	1.61±0.36	1.54±0.26	1.4±0.33	1.55±0.29	1.82±0.28	1.67±0.17	1.81±0.43	1.53±0.21	1.73±0.31	1.89±0.31*
IVSs (mm)	2±0.34	1.88±0.28	2.03±0.28	1.99±0.44	2.01±0.37	2.06±0.23	2.21±0.43	1.97±0.4	2.18±0.35	2.45±0.16*	2.56±0.4*	2.49±0.23*	2.51±0.38	2.62±0.43*
LVIDs (mm)	4±0.53	4.19±0.42	4.22±0.41	4.13±0.41	4.42±0.48	4.54±0.72	4.23±0.43	3.88±0.4	4.22±0.4	4.14±0.34	4.01±0.55	3.94±0.44	4.01±0.39	4.03±0.53
LVPWs (mm)	2.3±0.24	2.27±0.27	2.34±0.31	2.42±0.37	2.33±0.45	2.23±0.29	2.47±0.29	2.22±0.17	2.5±0.38	2.58±0.23	2.67±0.59**	2.41±0.16	2.63±0.36	2.67±0.46*
FS(%)	42.11±5.1	38.92±4.46	38.42±5.21	39.79±6.25	36.40±7.94	34.3±5.85	38.87±3.82	43.93±4.11	39.80±5.11	41.11±4.35	42.63±5.23	44.35±3.74	43.68±7.29	43.40±5.43
E wave velocity	92.9±11.31	99.67±5.31	90.42±11.88	91.68±9.34	95.03±9.55	96.38±14.58	97.72±16.27	96.88±11.01	95.33±16.99	102.67±7.23	94.67±8.12	101.53±11.2	101.76±19.3	110.67±23.6
E' IVS	6.1±1.71	6.13±1.21	5.68±1.05	5.45±1.09	6.43±1.88	5.34±0.77	5.4±1.1	5.23±0.65	6.4±1.83	6.92±1.2	4.78±1.26	6.01±1.09	5.15±1.16	6.23±1.52
E' FW	6.7±1.98	6.73±1.32	6.28±1.41	6.07±0.9	6.98±2.07	6.31±1.2	6.23±1.53	6.15±1.04	8.2±1.26**	7.17±1.66	5.98±1.28	7.19±2.03	5.95±1.85	7.72±1.93
DAP (mmHg)	51.42±5.57	53.5±6.26	58±13.72	54.67±6.02	53.58±9.35	57.3±14.16	56.17±7.91	54.25±19.99	56.5±12.8	63±8.54	70±13.51	67.67±10.14	70.3±10.61	59.33±12.46
MAP (mmHg)	66.19±4.9	68.75±3.54	72.28±9.62	67.14±6.12	67.92±6.52	69.3±10.5	72.11±5.15	69.08±17.6	74.25±8.65	77.57±6.71	84.47±10.41	80.25±14.7	85.6±11.9**	77.75±11.46
RWT	0.38±0.05	0.37±0.08	0.39±0.06	0.39±0.05	0.42±0.04	0.4±0.04	0.4±0.03	0.39±0.04	0.43±0.03	0.41±0.05	0.43±0.06	0.43±0.08	0.48±0.05	0.51±0.09*

\*p<0.05 and \*\* p<0.01 refer to the significance of the comparison along the study period (in weeks) in the HTN-CM and sham groups using two-way ANOVA, n=12. Values are expressed as mean  $\pm$ SD (n=12). IVSd, interventricular septum diastolic diameter; LVIDd, left ventricular internal diastolic diameter; LVPWd, left ventricular posterior wall diastolic diameter; IVSs, interventricular septum systolic diameter; LVIDs, left ventricular internal systolic diameter; LVPWs, left ventricular posterior wall systolic diameter; FS, fraction shortening; E wave velocity, the velocity of early mitral inflow; E' IVS, the early diastolic velocity of the septum; E' FW, the early diastolic velocity of the free wall; DAP, diastolic artery pressure; MAP, mean artery pressure; RWT, relative wall thickness.

Table 2-2. Evaluation of Salvianolic acid B and Carvedilol on conventional echocardiographic data in the investigated groups at the 4.5 and 6 weeks

Time	4.5 weeks				6 weeks			
Groups	Sham	HTN-CM	Sal B	Carvedilol	Sham	HTN-CM	Sal B	Carvedilol
IVSd (mm)	1.19±0.16	1.68±0.28	1.63±0.16	1.41±0.21	1.14±0.23	1.73±0.33**	1.57±0.19*	1.55±0.15
LVIDd (mm)	6.91±0.68	7.12±0.53	7.08±0.56	7.09±0.51	6.92±0.61	7.12±0.45	7.03±0.58	7.09±0.55
LVPWd (mm)	1.54±0.26	1.73±0.31	1.63±0.23	1.69±0.23	1.4±0.33	1.89±0.37	1.78±0.34	1.77±0.18
IVSs (mm)	2.06±0.23	2.51±0.38**	2.55±0.47**	2.26±0.20	2.21±0.43	2.62±0.48**	2.58±0.23**	2.36±0.21
LVIDs (mm)	4.54±0.72	4.01±0.39	4.06±0.47	4.14±0.51	4.23±0.43	4.03±0.33	3.8±0.52	3.93±0.6
LVPWs (mm)	2.23±0.29	2.63±0.36	2.52±0.44	2.64±0.41	2.47±0.29	2.67±0.23	2.77±0.54	2.75±0.34
FS (%)	34.3±5.85	43.68±7.29*	42.66±5.49	41.61±6.76	38.87±3.82	43.4±3.71	45.95±4.02	44.57±5.24
RWT	0.40±0.04	0.48±0.05	0.46±0.07	0.44±0.07	0.40±0.04	0.51±0.08*	0.48±0.06	0.47±0.05
E flow velocity	96.38±14.58	101.76±19.35	99.42±14.41	95.02±17.64	97.7±15.58	100.3±18.7	105.4±11.77	97.5±11.41
E' IVS	5.34±0.77	5.15±1.16	5.78±1.04	5.42±1.14	5.4±1.05	6.6±1.75*	5.4±0.87	5.5±0.49
E' FW	6.31±1.2	5.95±1.85	6.78±1.25	5.9±1.24	6.2±1.46	7±1.73	6.6±0.87	6.1±0.76
DAP (mmHg)	57.3±14.16	70.3±10.61	59.8±15.83	59±15.72	56.2±7.57	59.3±11.93	66.2±13.33	53.2±12.27
MAP (mmHg)	69.3±10.5	85.6±11.9**	73.9±13.08	71.4±12.56	72.1±4.93	77.8±10.97	79.5±11.84	70±11.57

\*p<0.05 and \*\* p<0.01 refer to the significance of the comparison between all groups using two-way ANOVA, n=12. Values are expressed as mean±SD (n=12). IVSd, interventricular septum diastolic diameter; LVIDd, left ventricular internal diastolic diameter; LVPWd, left ventricular posterior wall diastolic diameter; IVSs, interventricular septum systolic diameter; LVIDs, left ventricular internal systolic diameter; LVPWs, left ventricular posterior wall systolic diameter; FS, fraction shortening; E wave velocity, the velocity of early mitral inflow; E' IVS, the early diastolic velocity of the septum; E' FW, the early diastolic velocity of the free wall; DAP, diastolic artery pressure; MAP, mean artery pressure; RWT, relative wall thickness.

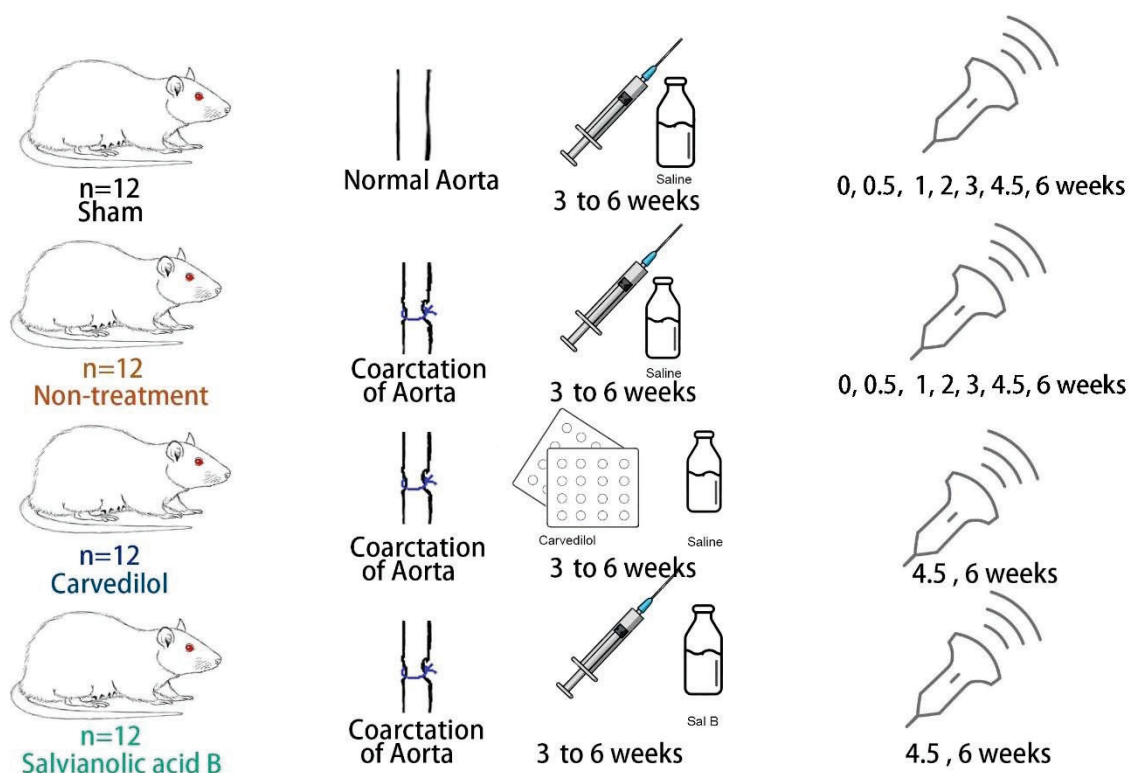


Figure.2-1 Schematic representation of experimental procedures and time frame of investigated groups

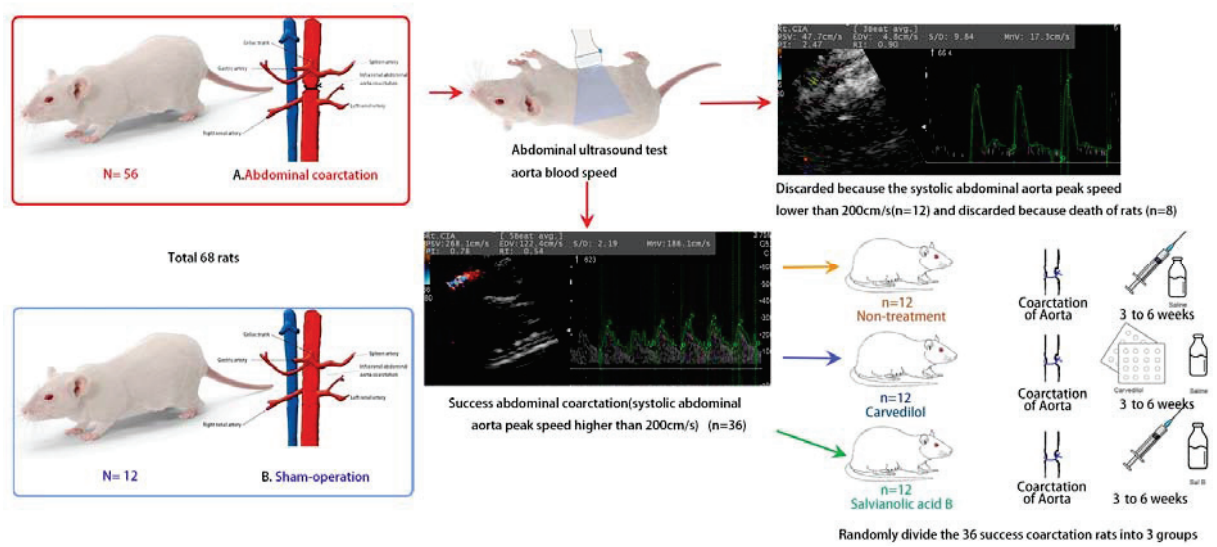


Figure.2-2 Abdominal coarctation surgery and discard criteria



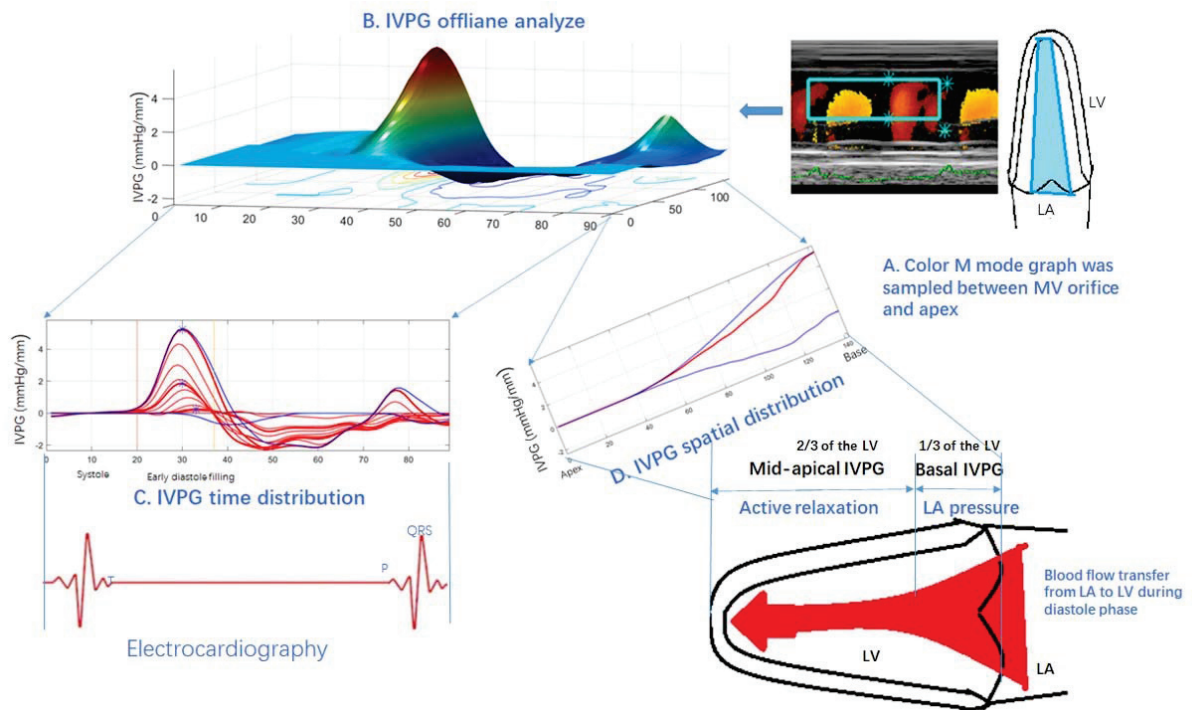


Figure.2-3 Procedures of IVPG analysis using the Euler equation by Matlab. Colour M-mode echocardiography was sampled (A) and then analyzed using Matlab (B), the time distribution (C), and spatial distribution of intraventricular pressure gradients were gained from the Matlab. The spatial distribution could be calculated into basal IVPG and mid-to-apical IVPG (D).

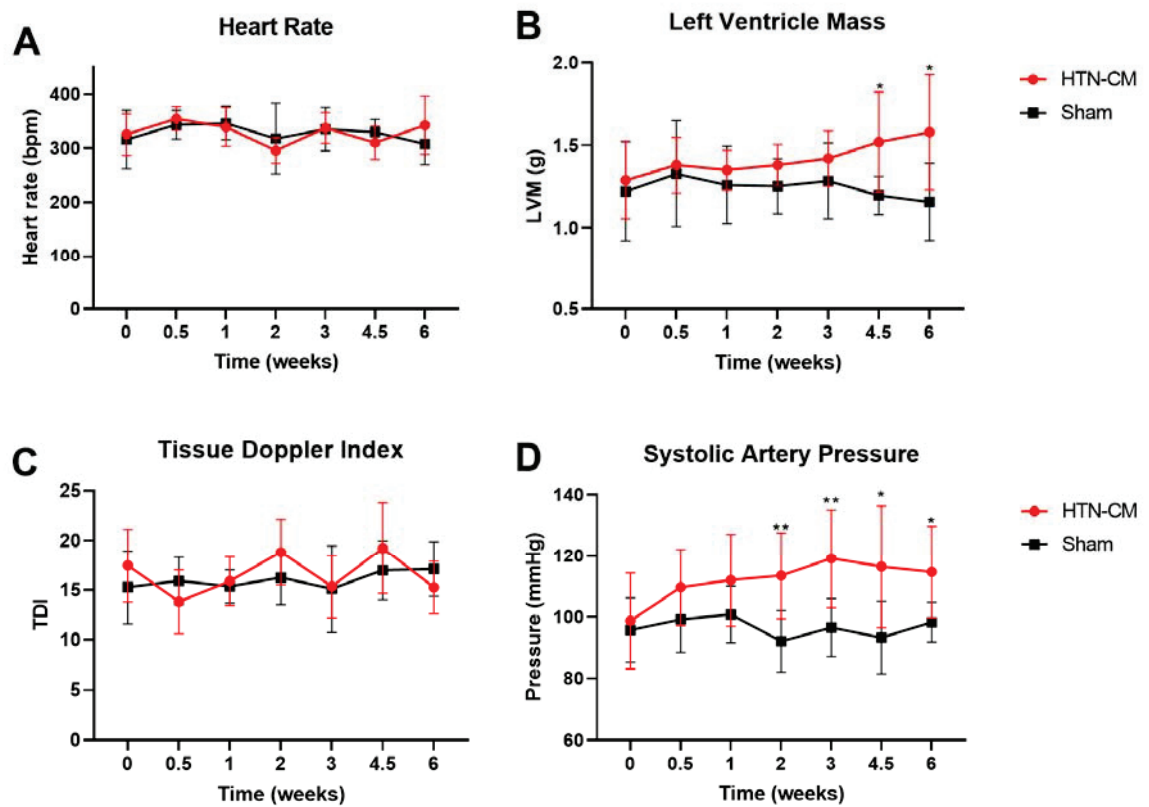


Figure.2-4 Basic measurements of the Sham group and HTN-CM group throughout the experimental intervals. \* $p < 0.05$  and \*\* $p < 0.01$  refer to comparisons between Sham and HTN-CM groups.

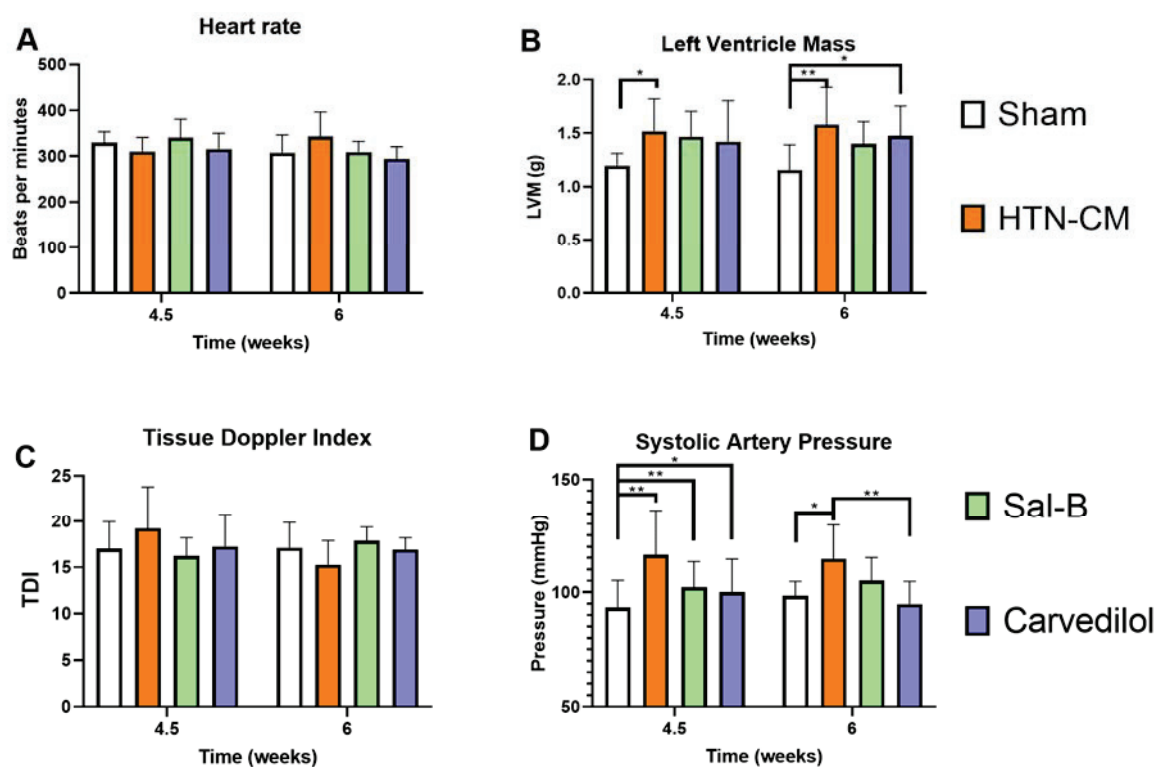


Figure.2-5 Basic measurements in all groups at 4.5 and 6 weeks.

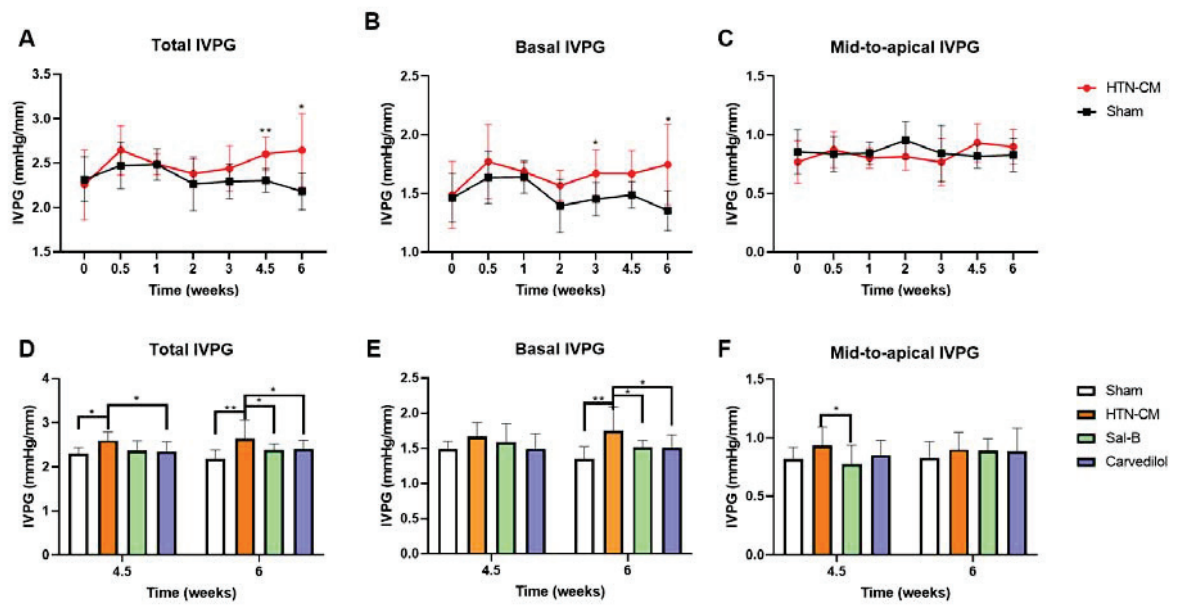


Figure.2-6 Comparison of IVPG results in different groups at different time intervals. A, B, & C graphs, respectively, represent the Total, Basal, and Mid-to-apical IVPG parts in Sham and HTN-CM groups throughout the entire experiment. D, E & F graphs, respectively, summarized the Total, Basal, and Mid-to-apical IVPG parts at 4.5 and 6 weeks in all groups. \* $p < 0.05$  and \*\*  $p < 0.01$  were used to compare the significance between groups.

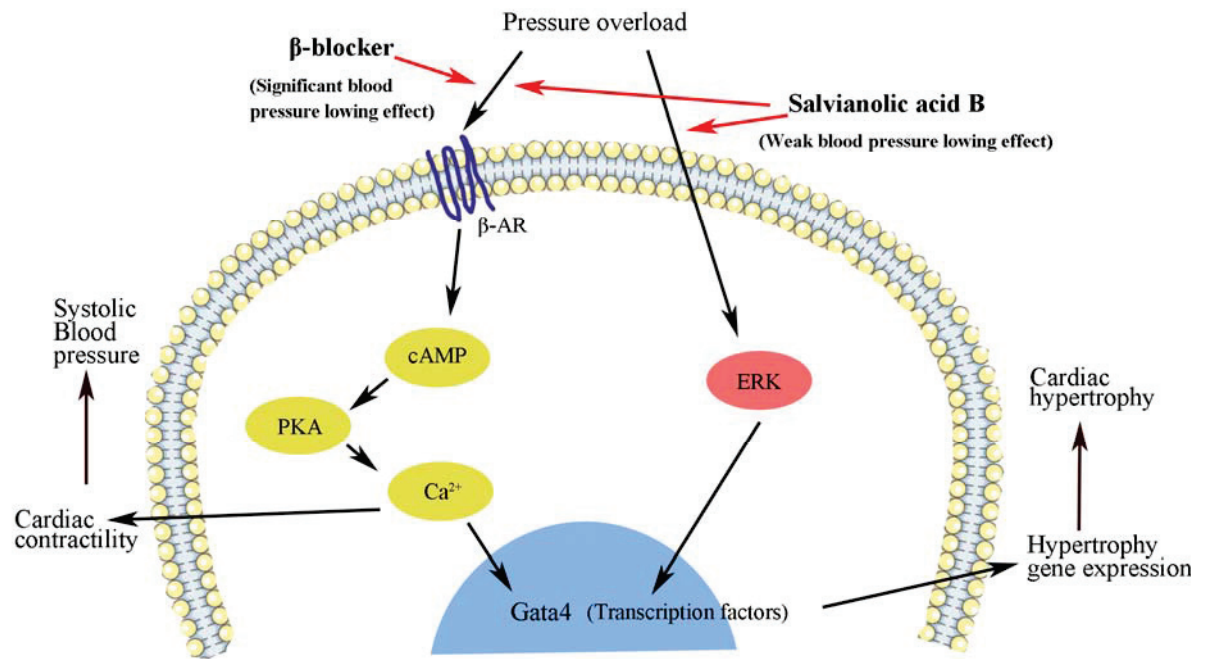


Figure.2-7 Sal-B and Carvedilol therapeutic pathway

Pressure overload activates the beta-adrenergic receptors and ERK, promote the expression of Gata4, result in hypertrophy. Sal B could inhibit the ERK and beta-adrenergic receptors at the same time while Carvedilol only works as a beta-blocker.

**Chapter 3**  
**Cardiac function change during the development in the complex pressure  
and volume overload model**

### 3.1 Introduction

Cardiovascular diseases (CVDs) are the leading cause of morbidity and mortality in renal failure patients(1). Left ventricle(LV) hypertrophy is the most prevalent cardiac disorder in these patients and LV hypertrophy was reported closely reported to higher mortality compared with patients without LV hypertrophy(90). After exploring the pathophysiology of pressure overload in chapter three, the need of understanding the pathophysiology of complex CVDs emerged as it can help clinicians identify and treat CVDs in patients originally from other system diseases including diabetes and urinary disease, as well as help patients prevent these potentially devastating complications. The purpose of this quantitative chapter is to explore the pathophysiology of uremic cardiomyopathy because pressure and volume overload are the main mechanisms of this disease.

Uremic cardiomyopathy (UC) refers to the cardiac disorder that is seen in patients with chronic kidney disease (CKD). Both pressure and volume overload were involved in the pathophysiology process of UC. UC characteristics as diastolic dysfunction disease that accompanies LV hypertrophy and fibrosis. Multiple factors including pressure and volume overload contribute to the pathogenesis of UC. Pressure overload occurs as a consequence of renal hypertension. The blood pressure typically rises with declines in renal function and this elevation of blood pressure eventually hastens the CKD progress. The volume overload occurs as a consequence of hypervolemia, as the progressive losing kidney function is not enough to maintain the osmotic status that eventually leads to volume expansion(91). The relationship between the different mechanisms and outcomes is still unclear. Also, the therapy that is effective in hypertensive cardiomyopathy only has a moderate effect on UC.

Among the multifactorial pathophysiology process in UC, LV hypertrophy is the result of pressure overload, volume overload, and the uremic state itself. Hypertension results in LV

pressure overload; LV volume overload occurs as a result of hypervolemia, anemia(92). Pressure overload led to concentric LV hypertrophy, while volume overload results in eccentric LV hypertrophy as shown in Figure. 3-1. LV hypertrophy is a beneficial adaptive response at the early stage of UC, but the continuing LV overload leads to maladaptive cardiomyocyte changes and cardiomyocyte death. The loss of cardiomyocytes leads to LV dilatation and eventually systolic dysfunction. Thus, the different types of LV hypertrophy may be observed in UC because pressure overload, volume overload, and uremic state affect LV differently. During the development of UC, the sympathetic activation and renin-angiotensin-aldosterone system (RAAS) were activated, which eventually led to elevated blood pressure. Hypervolemia caused by renal failure is a pathological condition in which there is too much fluid in the blood.

The renal mass reduction model is the most commonly used experimental model of CKD. The 5/6 subtotal nephrectomy technique was considered the best way to mimic human CKD in rats. After removing 5/6 of the nephron(93), the activation of RAAS combined with oxidative stress and inflammation in this model leads to glomerulosclerosis, tubulointerstitial injury, renal atrophy, and proteinuria, which exactly is the mechanism of human CKD (94). Thus, I consider this model as the proper approach in this study.

Currently, angiotensin-converting enzyme inhibitors (ACE-i) were considered as first-line therapeutic drugs in UC for their inhibition of RAAS. Because the use of ACE inhibitors is limited by their effects including hypotension, azotemia, and fatigue (95), scientists developed angiotensin receptor blockers (ARBs) with an expectation of better beneficial effects and fewer side effects on clinical endpoints. But ARBs have failed to demonstrate the same or better clinical effect, then scientists turn on herbal medicine, as it has been an effective poly chemical medical approach for centuries.



Salvianolic acid B (Sal B) was reported well a renoprotective effect in diverse kidney diseases, such as diabetic nephropathy, nephritis, and acute kidney injury (96, 97). Recently, reports indicate Sal B protects against renal fibrosis animals were published (98). Although Sal B could protect kidney fibrosis and prevent the Epithelial-mesenchymal transition process (99), the cardiovascular effect in hemodynamic and morphology of Sal B in cardiac disease caused by CKD is still unknown.

This chapter aims to evaluate the cardiac function change by intraventricular pressure gradients (IVPG) and speckle tracking echocardiography during the development of cardiac remodeling in uremic cardiomyopathy.

## **3.2 Materials and Methods**

### **3.2.1 Research design**

Abdominal artery coarctation and 5/6 subtotal nephrectomy were used for the induction of hypertensive cardiomyopathy(HTN) and uremic cardiomyopathy(UC). Both characteristics as LV hypertrophy, but the pathogenesis and affected location were different. Pressure overload is the main pathogenesis of HTN, while UC was dominant by pressure and volume overload at the same time.

The previous two studies showed the proper way to perform IVPG test and IVPG could reflect cardiac function change during the development of HTN-CM. The third experiment aims to evaluate cardiac function in a complex model, multiple factors and mechanisms were involved in the development of UC. Conventional echocardiography, IVPG, and speckle

tracking echocardiography were used to evaluate the change of anatomical and functional properties as previously performed.

### **3.2.2 Animal**

The experiments were carried in 36 female Sprague Dawley rats(Charles River Laboratories, Japan), aged 3 months, and weighing between 210 to 250 grams. According to Guide for the Care and Use of Laboratory Animals (1994), and with approval by the Institutional Animal Care and Use Committee of the Tokyo University of Agriculture and Technology. These rats have free access to food and water and are housed at 20 °C with a 12 hours light/dark cycle.

### **3.2.3 Induction of uraemic cardiomyopathy**

5/6 nephrectomy was performed on the UC and Sal B-UC group rats (n=12 and 12). In shorts, after pentobarbital (40mg/kg) intraperitoneal injection, the left kidney was exposed by a left laparotomy. The upper and lower kidney pole was cauterized, then the abdominal was closed. One week later, a total right nephrectomy was performed.

### **3.2.4 Sal B treatment**

The Sal B-UC group was treated with Sal B from the 4th to 8th-week post-operation. 5 mg/kg Sal B (Danshen DuofensuanYan 100mg, GreenValley Inc, Shanghai, China) was injected into the abdominal cavity after the rats were tightly caged. To decrease the disturbance

of injection to experiment result, the UC group rats received the same volume normal saline injection.

### **3.2.5 Echocardiography**

2, 4, 6, and 8 weeks after right nephrectomy, the rats underwent echocardiography. Isoflurane was used for induction and maintenance anesthesia because of its minimal effect on the heart rate (HR) and smooth recovery. Mask inhalation of 4% isoflurane with 1 L/min oxygen was used for induction. Then, rats were allowed to breathe spontaneously after reducing isoflurane to 2.5% for maintenance with 1 L/min oxygen. The whole echocardiography took approximately 40 min. All rats were performed echocardiography 2, 4, 6, and 8 weeks after right nephrectomy, the rats underwent echocardiography. The chest area was shaved, then electrocardiography leads were connected. An echocardiography machine (Hitachi Aloka Medical ProSound Premier 75CV, Japan) with a 12-MHz phased array probe was used and performed as described (100). Conventional echocardiography, Doppler of blood flow and tissue, diastolic colour Doppler M-mode (CDMM), and 2DTT were recorded five consecutive times and then averaged.

Myocardial velocities were obtained from pulsed-wave tissue Doppler imaging (TDI). The diastolic myocardial velocity ( $E'$ ) of the annulus was measured from both septal and lateral annuli. The diastolic CDMM images were captured and saved. The images were analyzed using the MATLAB software (The Mathworks, R2018b) with a specific equation designed for IVPG analysis.

The strain is a dimensionless measure of relative deformation that allows scientists to gain the myocardial movement on regional and global levels. This technique enables us to quantify strain rate, resulting in promising novel parameters of myocardial function. Loops of LV long

4 chamber axis view with a rate of 70 to 110 frames/s were acquired three times. The speckle-tracking analysis was performed by an algorithm incorporated into EchoPAC PC DAS-RSI (Hitachi Aloka Co., Tokyo, Japan) offline. The endocardial were traced manually at end-systole and end-diastole. The software algorithm automatically divided each imaging plane of LV into three equally circular sections: basal, midventricular, and apex on the septum and lateral as shown in Figure. 3. The longitudinal strain rate was obtained in totally six sections.

### **3.2.6 Blood sampling**

Blood sampling was performed at the 4 and 8 weeks in every rat. After I tightly caged the rat, 2 ml of blood was drowned from the tail vein. Blood samples were centrifuged at 3500 rpm for 5 min. The concentration of serum creatinine and blood urea nitrogen (BUN) were detected in each group by Dri-chem 7000V, Fujifilm, Tokyo, Japan).

### **3.2.7 Statistical analysis**

Data analysis was performed with a one-way analysis of variance (ANOVA) test with post hoc contrasts by Duncan test by using SPSS 21.0 (SPSS, Inc., Chicago, IL). For all studies, data are presented as mean  $\pm$  standard deviation. p Values less than .05 were considered statistically significant.

## **3.3 Results**

Polyuria was observed in the UC group from the 4, and swelling in the abdomen and limbs was observed from the 6 weeks, indicating hypervolemia. Table 1 illustrates the result

of cardiac morphology data of Sham operation, UC, and Sal B-UC rats. The systolic arterial blood pressure in UC rats was higher than in Sham rats from the 2 weeks ( $p<0.001$ ). UC group was higher than the Sham group in IVSd, LVPWd, IVSs, LVPWS, and FS. But LVIDd and LVIDs are lower in the UC group. Moreover, the LVM and RWT were increased in the UC rats in 2 and 4 weeks compared with the sham group. Based on these results, significant LV hypertrophy in UC rats was confirmed.

Besides, in the Sal B-UC group, the Sal B-UC group showed lower systolic, diastolic, and mean arterial blood pressure than the UC group but still higher than the Sham group. No difference between UC and Sal B-UC group was detected in IVSd, LVPWd, IVSs, LVPWS, FS, LVIDd, and LVIDs at 6 and 8 weeks. Also, the observed value of IVSd and LVPWd in the Sal B-UC treated group was less than the UC group but still greater than the sham group; meanwhile, IVSs, LVPWS, and FS were higher than the UC group.

Concentric hypertrophy was observed in the UC group at the 2, 6, and 8 weeks because the LVM and RWT were significantly higher than the sham group. It was noticed that in the UC group in the 4 weeks, the Sal B-UC groups showed eccentric hypertrophy at 6 and 8 weeks.

Hemodynamic parameters, IVPG, mitral inflow, and TDI data are summarized in Table 2. No difference was detected between Sham, UC, and Sal B groups in total, basal and mid-to-apical IVPG. Also, no significant difference was detected in E, E', and E/E' between these three groups.

The strain rate based on speckle tracking echocardiography were shown in Table 3. The UC and Sal B-UC group showed a significantly lower strain rate from 2 to 8 weeks compared with the sham group. In the UC group, once the strain rate was decreased in the mitral lateral segment, it did not show any promotion or diminishment. The strain rate decreased at 2 weeks

in the middle lateral segment, and further diminished myocardial function was observed at 4 weeks ( $p$  for time=0.202). In the other five segments, the  $p$  for time factor is less than 0.001, the strain rate in the UC group decreased compared with the sham group and it fluctuated during the development of UC. The Sal B-UC group showed a similar level of myocardial movement to the UC group.

Data of serum creatinine and BUN are presented in Tables 3-4. The data revealed a significant decrease in renal function tests in UC rats at the 2 and 4 weeks. Also, these biomarkers were significantly higher in the UC group than the Sal B-UC group; nevertheless, Sal B-UC was still higher than the sham group.

### **3.4 Discussion**

In the third experiment, the 5/6 subtotal nephrectomy method was used to producing an experimental model of UC, which was characterized by chronic kidney disease and cardiac dysfunction (92). CKD is a progressive pathological condition (101). I used the serum concentration of BUN and creatinine to estimate kidney function, which is the most prevalent kidney function evaluation technique. The 5/6 subtotal nephrectomy is the primary option for the investigation of CKD (102), not only because this model directly decreases the functional nephrons, but also this model showed clinical relevance (103).

The ventricular geometry in this experiment changed multiple times, the concentric hypertrophy (elevated RWT and LVM) was observed in UC rats at the 2, 6, and 8 weeks, but eccentric hypertrophy was observed in UC rats at the 4 weeks. This could be explained by the fact that multiple mechanisms are dominant at the different stages during the development of UC.

Patients with a different type of hypertrophy showed a different response to the same drugs, and this indicates different mechanisms dominants the eccentric and concentric hypertrophy (104). In concentric LV hypertrophy, the sympathetic nervous system is overactivated. Activation of beta-adrenoceptor in the heart results in cardiomyocyte hypertrophy and progressive heart failure (105). And it was considered as the main mechanism of concentric hypertrophy (106). Sal B was believed to own a similar mechanism as beta-blocker, which is the first-line therapeutic drug in concentric hypertrophy (Figure. 3-4). Previously, I proved that Sal B has protective effects in concentric LV hypertrophy caused by pressure overload, Sal B prevented further development of hypertrophy without pressure lowering effect (107). In this chapter, Sal B showed a therapeutic effect of UC, after the injection of Sal B, the concentric hypertrophy was not observed at the 6 and 8 weeks, while the UC group rats showed significantly higher RWT. Thus, it was believed that the mechanism inducing concentric hypertrophy was blocked by Sal B.

The RAAS plays a crucial role in signalling pathways that are involved in the pathogenesis of renal hypertension and cardiac remodeling. After the angiotensin II receptor was activated, the protein kinase C (PKC) was stimulated, which in turn activates the mitogen-activated protein kinase (MAPKs) pathway (108). The activation of the MARKs family leads to cardiac remodeling (108). ACE-I and ARB could block the RAAS pathways. Sal B was reported to affect to alleviate angiotensin II-induced cardiac fibrosis(109), which indicates that Sal B could block RAAS pathways(figure 3-4).

Strain rate is the change in deformation at a specific time. Strain-based imaging also called speckle tracking echocardiography is a noninvasive echocardiography technique that tracks myocardial deformation. The ventricular strain is an accurate measure of myocardial dysfunction. Subclinical myocardial dysfunction was detected in early-stage CKD patients, which correlates with cardiomyopathy, congestive heart failure, and mortality (110).

The myocardial function was evaluated in this experiment, the myocardial dysfunction occurs from the 2 weeks till the 8 weeks, and the Sal B also did not reverse the decreased longitudinal strain rate at the 6 and 8 weeks. The hypertrophy in UC rats was not apparent until the 6 weeks, which implies the myocardial dysfunction occurs before changes in ventricular geometry (111). In this experiment, the HR was gain under anesthesia, and the anesthesia was equal to all rats, thus the HR could be considered as resting HR. Similar results were also observed in the HR, the HR in the UC group higher than the sham group at every time point. The elevated resting HR correlates with a higher risk of death (112), which indicates that cardiac function in the UC group was damaged and the damage was not reversed by using Sal B.

No difference was detected among groups by IVPG. Scientists proved that basal IVPG correlates with E wave velocity and mid-to-apical IVPG correlates with myocardial movement(31). The newest guideline of LV diastolic function indicates that E/E' is the crucial part of the staging algorithm of diastolic dysfunction (113). Combine with the fact that the E wave velocity, E' and E/E' also showed no difference between groups, it is easy to come out with the conclusion that the LA pressure was not elevated in the UC group.

The main difference in mechanism in forming concentric and eccentric hypertrophy is the mechanical stress stimuli to the ventricle wall(104, 114). The ventricular morphology changed means that the mechanical stress fluctuates during the development of UC. The myocardial dysfunction occurred in the UC group from 2 to 8 weeks, the LV mass and RWT fluctuated, these eventually lead to a fluctuated but not a significantly different level of active relaxation in the UC group confirmed by mid-to-apical IVPG.

The CKD was confirmed in UC rats by the elevated BUN and creatinine from the 2 weeks till the endpoint of monitoring. And the Sal B showed treatment effect by reversing the



elevated BUN and creatinine at the 6 and 8 weeks. The damaged kidney function was ameliorated by Sal B through reducing epithelial-mesenchymal transition-related proteins(99). The epithelial-mesenchymal transition in the process of renal fibrosis was promoted by Sal B through activating autophagy mediated by Sirt1(99).

### **3.5 Limitation**

The urinary creatinine to serum creatinine (UCr/SCr) ratio is useful indices of renal damage, but it was not used in this experiment, because the urine of rats was not collected. Due to lacking the budget to purchase metabolism cages for rats and invasiveness of repeat urine sampling by syringe.

But this defect may not interfere with the credibility of the experiment, because current kidney function evaluation may be enough. After all, the kidney function was not changed dramatically after the initial ablation of the kidney.

### **3.6 Conclusion**

Myocardial dysfunction occurs before morphological ventricular changes during the development of UC, both eccentric and concentric hypertrophy was observed in UC. Sal B could prevent further development in UC, and partially protect against kidney injury in CKD. LA pressure and active relaxation were not changed during the development of UC.

Table 3-1. The baseline cardiac morphology and data of Sham operation, UC and SalB treated rats

time	2 weeks		4 weeks		6 weeks			8 weeks			<i>P</i> of time	<i>P</i> of group	<i>P</i> of interaction
Group	sham	UC	sham	UC	sham	UC	Sal B-UC	sham	UC	Sal B-UC			
SAP	104.14±10.68 <sup>b</sup>	115.86±5.59 <sup>c</sup>	103.21±5.19 <sup>ab</sup>	124.63±12.6 <sup>cde</sup>	93.41±15 <sup>a</sup>	133.58±13.56 <sup>e</sup>	121.24±9.45 <sup>cd</sup>	100.53±15.25 <sup>ab</sup>	144.12±11.98 <sup>f</sup>	126.75±11.21 <sup>de</sup>	0.002**	0.000**	0.000**
DAP	78.6±18.95 <sup>ab</sup>	80.29±4.49 <sup>ab</sup>	74.26±6.38 <sup>a</sup>	98.48±10.75 <sup>c</sup>	73.75±6.55 <sup>a</sup>	104.13±9.8 <sup>c</sup>	88.59±9.82 <sup>b</sup>	73.2±5.63 <sup>a</sup>	123.93±19.57 <sup>d</sup>	106.18±14.43 <sup>c</sup>	0.000**	0.000**	0.000**
MAP	87.11±15.24 <sup>ab</sup>	92.15±2.43 <sup>b</sup>	83.91±4.91 <sup>a</sup>	107.2±9.64 <sup>c</sup>	80.3±6.17 <sup>a</sup>	113.94±8.08 <sup>cd</sup>	110.36±7.15 <sup>c</sup>	82.31±8.05 <sup>a</sup>	130.66±13.52 <sup>e</sup>	119.89±8.4 <sup>d</sup>	0.000**	0.000**	0.000**
IVSd	1.12±0.1 <sup>a</sup>	1.5±0.31 <sup>cde</sup>	1.13±0.12 <sup>a</sup>	1.36±0.22 <sup>bc</sup>	1.21±0.17 <sup>ab</sup>	1.57±0.35 <sup>de</sup>	1.39±0.26 <sup>bcd</sup>	1.3±0.16 <sup>ab</sup>	1.67±0.3 <sup>e</sup>	1.57±0.15 <sup>de</sup>	0.001**	0.000**	0.670
LVIDd	7.36±0.72 <sup>b</sup>	6.58±1.47 <sup>a</sup>	7.71±0.68 <sup>b</sup>	7.67±0.55 <sup>b</sup>	7.53±0.62 <sup>b</sup>	7.32±0.27 <sup>b</sup>	7.93±0.5 <sup>b</sup>	7.25±0.58 <sup>b</sup>	7.32±0.54 <sup>b</sup>	7.87±0.69 <sup>b</sup>	0.017*	0.000**	0.743
LVPWd	1.43±0.25 <sup>ab</sup>	1.72±0.35 <sup>bc</sup>	1.4±0.21 <sup>ab</sup>	1.43±0.26 <sup>ab</sup>	1.32±0.27 <sup>a</sup>	1.78±0.54 <sup>c</sup>	1.43±0.36 <sup>a</sup>	1.64±0.33 <sup>abc</sup>	1.95±0.53 <sup>c</sup>	1.49±0.46 <sup>c</sup>	0.016*	0.000**	0.402
IVSs	1.88±0.28 <sup>ab</sup>	2.57±0.43 <sup>ef</sup>	1.79±0.32 <sup>a</sup>	2.21±0.48 <sup>bcde</sup>	2.06±0.39 <sup>abc</sup>	2.29±0.55 <sup>cdef</sup>	2.16±0.46 <sup>abcd</sup>	1.96±0.4 <sup>abc</sup>	2.5±0.52 <sup>def</sup>	2.63±0.19 <sup>f</sup>	0.042*	0.000**	0.101
LVIDs	4.19±0.42 <sup>bc</sup>	3.74±0.4 <sup>a</sup>	4.38±0.56 <sup>bc</sup>	4.25±0.86 <sup>bc</sup>	4.34±0.5 <sup>bc</sup>	4.25±0.38 <sup>bc</sup>	4.48±0.36 <sup>c</sup>	4.36±0.46 <sup>bc</sup>	3.93±0.51 <sup>ab</sup>	4.13±0.44 <sup>abc</sup>	0.028*	0.029*	0.524
LVPWs	2.27±0.27 <sup>a</sup>	2.51±0.4 <sup>a</sup>	2.21±0.34 <sup>a</sup>	2.24±0.16 <sup>a</sup>	2.32±0.32 <sup>a</sup>	2.55±0.72 <sup>ab</sup>	2.39±0.18 <sup>a</sup>	2.38±0.43 <sup>a</sup>	2.88±0.68 <sup>bc</sup>	2.95±0.44 <sup>c</sup>	0.001**	0.009**	0.172
FS	42.54±4.46 <sup>ab</sup>	46.63±4.29 <sup>bc</sup>	43.22±4.55 <sup>abc</sup>	44.97±8.2 <sup>bc</sup>	42.59±4.63 <sup>ab</sup>	41.78±4.99 <sup>ab</sup>	43.58±4.19 <sup>abc</sup>	39.59±7.6 <sup>a</sup>	46.45±5.41 <sup>bc</sup>	47.67±3.28 <sup>c</sup>	0.185	0.003**	0.093
LVM	0.6±0.08 <sup>a</sup>	0.68±0.13 <sup>ab</sup>	0.64±0.07 <sup>ab</sup>	0.73±0.15 <sup>abc</sup>	0.62±0.11 <sup>ab</sup>	0.91±0.34 <sup>cd</sup>	0.79±0.23 <sup>abc</sup>	0.71±0.11 <sup>abc</sup>	0.99±0.38 <sup>cd</sup>	0.86±0.24 <sup>cd</sup>	0.008**	0.000**	0.471
RWT	0.35±0.07 <sup>c</sup>	0.46±0.09 <sup>ab</sup>	0.33±0.05 <sup>c</sup>	0.38±0.07 <sup>bc</sup>	0.34±0.07 <sup>c</sup>	0.46±0.13 <sup>ab</sup>	0.36±0.07 <sup>c</sup>	0.41±0.07 <sup>abc</sup>	0.49±0.09 <sup>a</sup>	0.39±0.06 <sup>bc</sup>	0.000**	0.000**	0.468

Echocardiographic measurements in sham, UC, and Sal B-UC group rats. Two-way ANOVA was performed to test the difference between groups and time points, Turkey test was used for post hoc comparison. SAP, systolic arterial pressure; DAP, diastolic arterial pressure; MAP, mean arterial pressure; IVSd, interventricular septum diastolic diameter; LVIDd, left ventricular internal diastolic diameter; LVPWd, left ventricular posterior wall diastolic diameter; IVSs, interventricular septum systolic diameter; LVIDs, left ventricular internal systolic diameter; LVPWs, left ventricular posterior wall systolic diameter; FS, fraction shorting; LVM, left ventricle mass; RWT, relative wall thickness.

<sup>abcd</sup> were used for consistent subset classification, for instance, xx.xx<sup>a</sup> is different with yy.yy<sup>b</sup> because a and b illustrate that they belong to different subset, but yy.xx<sup>ab</sup> did not significant different compare with yy.yy<sup>b</sup> because they belong to 'b', the same subset.  $P < 0.05$  was considered as the significance level.

Table 3-2. IVPG and TDI in uraemic cardiomyopathy, sham operation, and Sal B-treated rats

time	2 weeks		4 weeks		6 weeks			8 weeks			P of time	P of group	P of interaction
Group	sham	UC	sham	UC	sham	UC	Sal B-UC	sham	UC	Sal B-UC			
Total IVPG	2.46±0.27 <sup>b</sup>	2.29±0.22 <sup>ab</sup>	2.26±0.26 <sup>ab</sup>	2.46±0.15 <sup>b</sup>	2.18±0.25 <sup>a</sup>	2.28±0.22 <sup>ab</sup>	2.3±0.25 <sup>ab</sup>	2.31±0.3 <sup>ab</sup>	2.43±0.3 <sup>b</sup>	2.42±0.29 <sup>b</sup>	0.089	0.316	0.125
Basal IVPG	1.5±0.25 <sup>b</sup>	1.35±0.12 <sup>ab</sup>	1.42±0.19 <sup>ab</sup>	1.46±0.18 <sup>ab</sup>	1.31±0.16 <sup>a</sup>	1.43±0.12 <sup>ab</sup>	1.44±0.24 <sup>ab</sup>	1.41±0.29 <sup>ab</sup>	1.36±0.13 <sup>ab</sup>	1.46±0.13 <sup>ab</sup>	0.480	0.275	0.190
Mid-to-apical IVPG	0.97±0.14 <sup>ab</sup>	0.93±0.16 <sup>ab</sup>	0.84±0.14 <sup>a</sup>	1±0.19 <sup>ab</sup>	0.87±0.14 <sup>a</sup>	0.86±0.16 <sup>a</sup>	0.86±0.26 <sup>a</sup>	0.9±0.14 <sup>ab</sup>	1.07±0.32 <sup>b</sup>	0.96±0.31 <sup>ab</sup>	0.117	0.234	0.291
E	99.58±13.48 <sup>ab</sup>	98.5±13.39 <sup>abd</sup>	91.23±10.82 <sup>a</sup>	110.57±8.85 <sup>b</sup>	105.58±17.51 <sup>b</sup>	106.49±10.79 <sup>bd</sup>	103.26±14.52 <sup>ab</sup>	97.71±16.91 <sup>ab</sup>	106.47±16.2 <sup>bd</sup>	99.83±19.44 <sup>abd</sup>	0.351	0.054	0.128
HR	330.49±32.05 <sup>abc</sup>	358.33±29.3 <sup>cd</sup>	310.71±35.46 <sup>ab</sup>	346.34±38.94 <sup>bcd</sup>	298.74±47.14 <sup>a</sup>	378±56.29 <sup>d</sup>	353.03±42.92 <sup>cd</sup>	310.23±50.05 <sup>ab</sup>	375.72±45.1 <sup>d</sup>	364.51±45.82 <sup>cd</sup>	0.510	0.000**	0.218
E'	5.69±0.65 <sup>ab</sup>	6.04±1.23 <sup>b</sup>	5.71±0.66 <sup>ab</sup>	5.57±0.39 <sup>ab</sup>	5.18±1.06 <sup>a</sup>	6.32±1.42 <sup>b</sup>	6.06±1.09 <sup>b</sup>	5.48±0.6 <sup>ab</sup>	6.16±0.77 <sup>b</sup>	5.62±0.53 <sup>ab</sup>	0.799	0.024	0.108
E/E'	16.64±1.17 <sub>a</sub>	16.72±1.45 <sup>a</sup>	16.45±2.58 <sup>a</sup>	20.01±1.6 <sup>b</sup>	16.75±4.12 <sup>a</sup>	17.76±3.87 <sup>ab</sup>	17.45±2.99 <sup>a</sup>	16.69±2.21 <sup>a</sup>	17.73±3.51 <sup>ab</sup>	17.97±3.14 <sup>ab</sup>	0.293	0.042*	0.279

Echocardiographic measurements in sham, UC, and Sal B-UC group rats. two-way ANOVA was performed to test the difference between groups and time

points, Turkey test was used for post hoc comparison. Total IVPG, the mix of basal and mid-to-apical intraventricular pressure gradients; basal IVPG, the basal intraventricular pressure gradients; mid-to-apical IVPG, the mid plus apex intraventricular pressure gradients; E, the velocity of early mitral inflow; HR, heart rate; E', Peak velocity of early diastolic mitral annular motion as determined by pulsed-wave Doppler; E/E', Ratio of E to E'.

<sup>abcd</sup> were used for consistent subset classification, for instance, xx.xx<sup>a</sup> is different with yy.yy<sup>b</sup> because a and b illustrate that they belong to different subsets,

but yy.xx<sup>ab</sup> did not significant different compare with yy.yy<sup>b</sup> because they belong to 'b', the same subset. P < 0.05 was considered as the significance level.

Table 3-3. Strain rate in uraemic cardiomyopathy, sham operation, and Sal B-treated rats

time	2 weeks		4 weeks		6 weeks			8 weeks			<i>P</i> of time	<i>P</i> of group	<i>P</i> of interaction
Group	sham	UC	sham	UC	sham	UC	Sal B-UC	Sham	UC	Sal B-UC			
APS	3.83±0.41 <sup>a</sup>	2.39±0.3 <sup>c</sup>	3.72±0.37 <sup>a</sup>	2.58±0.47 <sup>bc</sup>	4.19±0.41 <sup>a</sup>	2.97±0.41 <sup>b</sup>	3.12±0.51 <sup>b</sup>	4.08±0.48 <sup>a</sup>	3.04±0.4 <sup>b</sup>	2.68±0.3 <sup>bc</sup>	0.000 <sup>**</sup>	0.000 <sup>**</sup>	0.144
MS	14.64±1.58 <sup>a</sup>	6.89±0.8 <sup>d</sup>	13.58±1.36 <sup>a</sup>	8.8±1.38 <sup>c</sup>	11.35±1.12 <sup>b</sup>	7.81±1.09 <sup>cd</sup>	8.3±1.36 <sup>cd</sup>	13.51±1.6 <sup>a</sup>	8.9±1.17 <sup>c</sup>	8.64±0.96 <sup>c</sup>	0.000 <sup>**</sup>	0.000 <sup>**</sup>	0.000 <sup>**</sup>
BS	10.28±1.11 <sup>cd</sup>	7.5±0.9 <sup>e</sup>	18.84±1.88 <sup>a</sup>	7.07±1.14 <sup>e</sup>	11.97±1.19 <sup>b</sup>	7.5±1.05 <sup>e</sup>	9.29±1.52 <sup>d</sup>	11.5±1.36 <sup>bc</sup>	7.08±0.93 <sup>e</sup>	7.5±0.84 <sup>e</sup>	0.000 <sup>**</sup>	0.000 <sup>**</sup>	0.000 <sup>**</sup>
APL	7.96±0.86 <sup>a</sup>	6.21±0.94 <sup>cd</sup>	6.31±0.63 <sup>c</sup>	6.1±0.87 <sup>cd</sup>	6.81±0.67 <sup>bc</sup>	6.55±0.91 <sup>bc</sup>	6.79±1.11 <sup>bc</sup>	7.45±0.88 <sup>ab</sup>	5.12±0.67 <sup>d</sup>	7.05±0.79 <sup>abc</sup>	0.003 <sup>**</sup>	0.000 <sup>**</sup>	0.000 <sup>**</sup>
ML	10.27±1.11 <sup>a</sup>	5.92±0.66 <sup>c</sup>	9.65±0.96 <sup>ab</sup>	6.32±0.64 <sup>c</sup>	8.65±0.86 <sup>b</sup>	6.55±0.91 <sup>c</sup>	6.23±1.02 <sup>c</sup>	9.23±1.09 <sup>ab</sup>	6.19±0.81 <sup>c</sup>	6.05±0.67 <sup>c</sup>	0.202	0.000 <sup>**</sup>	0.001 <sup>**</sup>
BL	9.02±0.97 <sup>b</sup>	7.78±1 <sup>c</sup>	8.02±0.8 <sup>bc</sup>	5.01±0.68 <sup>e</sup>	10.68±1.06 <sup>a</sup>	5.86±0.82 <sup>de</sup>	7.48±1.23 <sup>c</sup>	7.72±0.92 <sup>c</sup>	7.23±0.95 <sup>c</sup>	7.05±0.79 <sup>cd</sup>	0.000 <sup>**</sup>	0.000 <sup>**</sup>	0.000 <sup>**</sup>

Longitudinal strain rate in sham, UC, and Sal B-UC group rats. APS, the apical segment of the septum; MS, the middle segment of the septum; BS, the basal segment of the septum; APL, the apical segment of the lateral free wall; ML, the middle segment of the lateral free wall; BL, the basal segment of the lateral free wall.

<sup>abcd</sup> were used for consistent subset classification, for instance, xx.xx<sup>a</sup> is different with yy.yy<sup>b</sup> because a and b illustrate that they belong to different subset, but yy.xx<sup>ab</sup> did not significant different compare with yy.yy<sup>b</sup> because they belong to 'b', the same subset.  $P < 0.05$  was considered as the significance level.

Table 3-4. Kidney function evaluation in uraemic cardiomyopathy, sham operation, and Sal B-treated rats

time	2 weeks		4 weeks		6 weeks			8 weeks			<i>P</i> of	<i>P</i> of	<i>P</i> of
Group	sham	UC	sham	UC	sham	UC	Sal B-UC	sham	UC	Sal B-UC	time	group	interaction
Creatinine (mg/dL)	0.5±0.05 <sup>d</sup>	1.49±0.19 <sup>b</sup>	0.53±0.06 <sup>d</sup>	1.8±0.23 <sup>ab</sup>	0.53±0.06 <sup>d</sup>	1.91±0.25 <sup>a</sup>	1.27±0.19 <sup>c</sup>	0.49±0.05 <sup>d</sup>	1.87±0.24 <sup>a</sup>	1.24±0.19 <sup>c</sup>	0.000 <sup>**</sup>	0.000 <sup>**</sup>	0.001 <sup>**</sup>
BUN (mg/dL)	37.97±5.73 <sup>d</sup>	120.19±15.97 <sup>ab</sup>	38.94±5.88 <sup>d</sup>	125.19±16.64 <sup>a</sup>	36.99±5.59 <sup>d</sup>	128.2±17.03 <sup>a</sup>	104.26±9.67 <sup>bc</sup>	39.43±5.96 <sup>d</sup>	132.17±21.09 <sup>a</sup>	102.37±9.49 <sup>c</sup>	0.408	0.000 <sup>**</sup>	0.516

Kidney function evaluation in sham, UC, and Sal B-UC group rats. One-way ANOVA was performed to test the difference between groups and time points, Turkey test was used for post hoc comparison.

<sup>abcd</sup> were used for consistent subset classification, for instance, xx.xx<sup>a</sup> is different with yy.yy<sup>b</sup> because a and b illustrate that they belong to different subsets, but yy.xx<sup>ab</sup> did not significant different compare with yy.yy<sup>b</sup> because they belong to ‘b’, the same subset.  $P < 0.05$  was considered as the significance level.

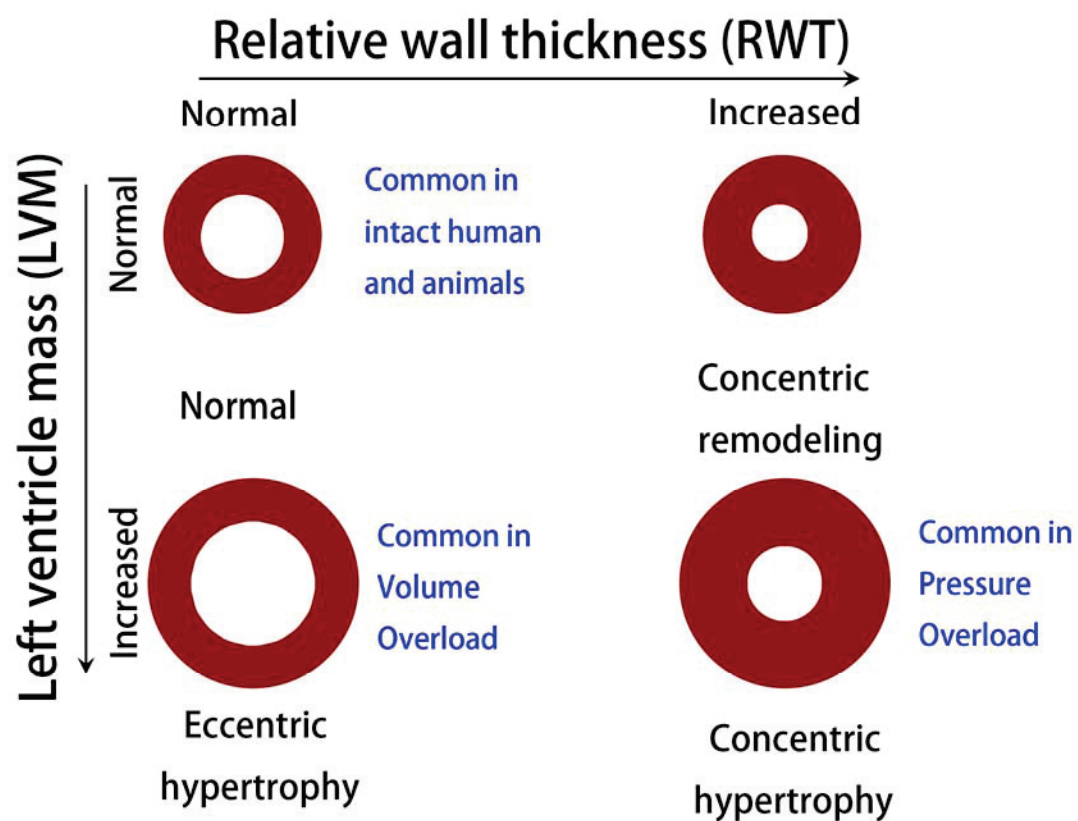


Figure.3-1 Basic pattern of left ventricular remodeling.

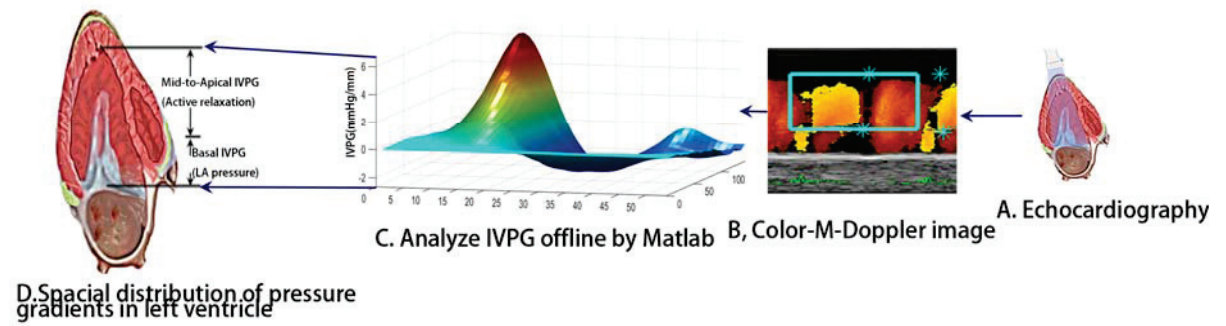


Figure.3-2 IVPG analysis with the Euler equation by Matlab



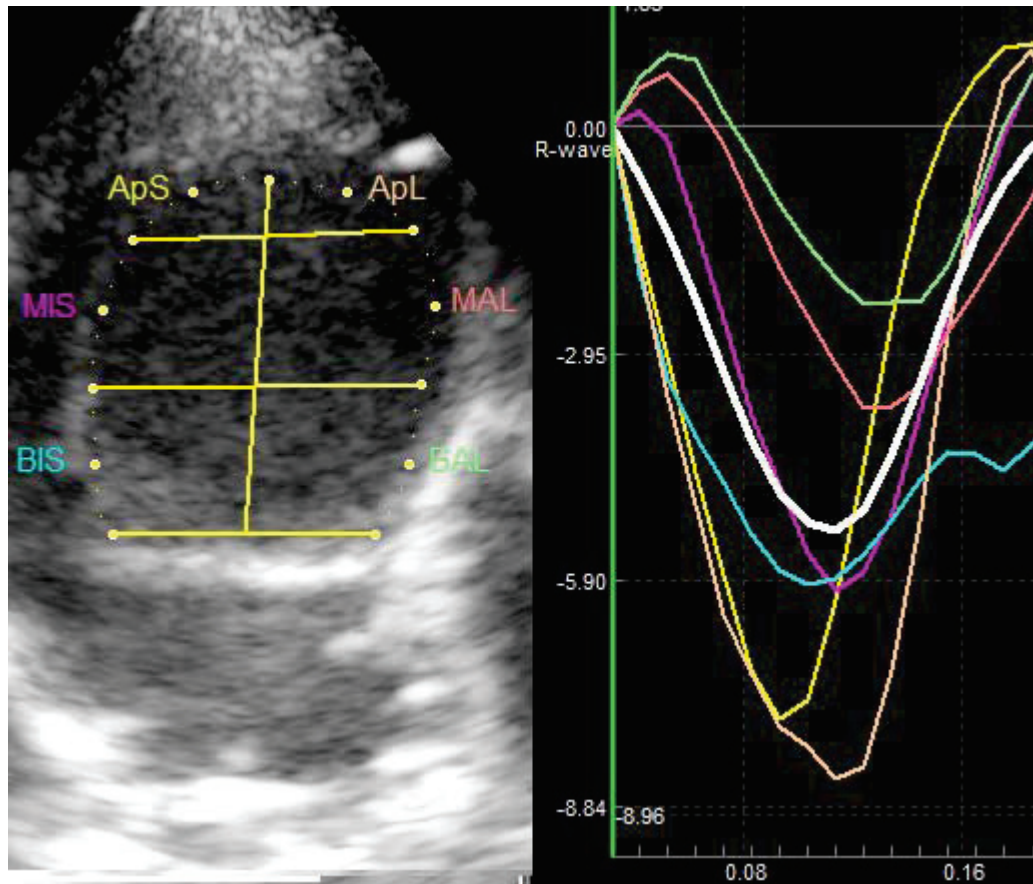


Figure.3-3 Speckle tracking echocardiography

Left: segmentation of the left ventricle APS, the apical segment of the septum; MS, the middle segment of the septum; BS, the basal segment of the segment; APL, the apical segment of the lateral free wall; ML, the middle segment of the lateral free wall; BL, the basal segment of the lateral free wall.

Right: Strain rate of each segment

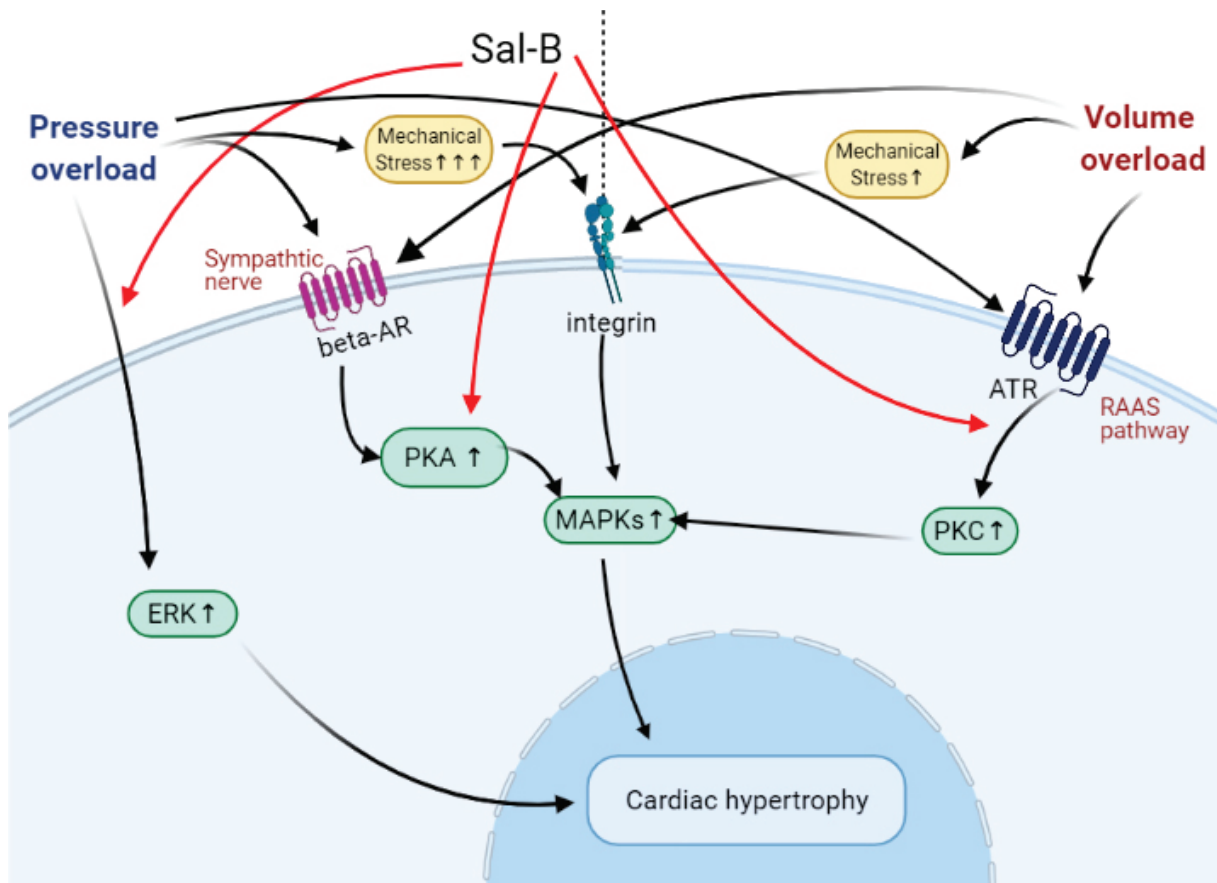


Figure.3-4 Pathogenesis during the development of UC, both pressure and volume overload was dominant in a different stage

The red arrow indicates the Sal B blocked this pathway. Beta-AR, beta-adrenergic receptor; ATR, angiotensin receptor; MAPKs, mitogen-activated protein kinase; PKC, protein kinase C; ERK, extracellular signal-regulated kinases.

## **General Conclusion**

Cardiovascular diseases are the leading cause of humans and animals. Echocardiography is the ultrasound specific for the heart, it was used to evaluate cardiac function noninvasively *in vivo*. But the conventional echocardiography not only was interfered with by many factors like heart rate, and mitral inflow pattern but also it was cannot directly evaluate diastolic function. Thus, scientists developed novel echocardiography techniques like intraventricular pressure gradients to evaluate cardiac function.

The present thesis was designed to provide a further understanding of the pathophysiology of CVDs and the treatment effect of the medicine.

In the first chapter, I used a group of rats with or without LV hypertrophy to investigate the principle of performing IVPG, which is a parameter that evaluates the cardiac function noninvasively without the effect of preload. From this experiment, it was concluded that intentionally control heart rate in performing echocardiography is not necessary.

In the second chapter, I produced a hypertensive cardiomyopathy model, which is the pressure overload model. The abdominal coarctation was performed to induce an elevated vascular resistance, which leads to hypertension and consecutive cardiac remodeling. Concentric hypertrophy and elevated basal IVPG were observed in the HTN-CM model. The change of IVPG occurs before the morphologic change, and the Sal B showed therapeutic effect by diminishing the elevated basal IVPG and prevent further development of concentric hypertrophy.

In the third chapter, I produced complex uremic cardiomyopathy (UC) model, which is the combination of pressure overload and volume overload. The 5/6 subtotal nephrectomy was performed to produce a UC model. During the development of UC, we found out that myocardial dysfunction occurs before morphological changes during the development of UC. And we confirmed the kidney dysfunction in the UC model, and Sal B reversed the elevated

creatinine and blood urea nitrogen. Both concentric and eccentric hypertrophy was observed in the UC model. Sal B prevents the further development of concentric hypertrophy in the uremic cardiomyopathy model. Both pressure and volume overload are dominant in different stages of uremic cardiomyopathy.

Conventional echocardiography is failed in distinguishing regional cardiac function and is easy to affect by heart rate and mitral inflow patterns. Therefore, IVPG and speckle-tracking echocardiography have been developed to provide a more accurate investigation of the heart's cardiac function. By minimizing the limitation of conventional echocardiography, IVPG can be used as a useful index to evaluate the cardiac performance regionally and globally, which can be evaluated into different heart segments such as apical, middle, or basal parts.

This study can conclude that the cardiac functional and morphological changes occurred at different times during the development of cardiac remodeling. The HTN-CM showed concentric hypertrophy while the uremic cardiomyopathy showed eccentric and concentric hypertrophy at different time points. Sal B has a treatment effect in HTN-CM and UC. Sal B could prevent the development of hypertrophy caused by pressure overload. The result of this thesis explored the pathophysiology during the development of cardiac remodeling in the simple and complex model, this pathophysiology information is beneficial to human and veterinary cardiology study of pathophysiology which eventually helps physicians and veterinarians in clinical to provide higher quality health services for human and animals, eventually contribute to the harmonization of nature and society.

## **Study limitation**

The present study was designed to provide a further understanding of the pathophysiology of CVDs and the treatment effect of the medicine. Catheterization provides accurate pressure,

volume, and pressure-volume relationship at the systole and diastole phases which is the golden standard of cardiac function. However, the invasiveness limited its repeated use that it is hard to close monitoring the cardiac function change.

Thus, I did not confirm the pressure and volume overload directly by the catheterization, the pressure overload was confirmed by blood pressure monitoring and the volume overload was confirmed by the kidney dysfunction and hypervolemia.

Also, the effect of heart rate was not manipulated by the pacemaker in chapter two, as the pacemaker can only increase the heart rate and electrocardiography will be interfered with by the pacemaker.

## **Acknowledgment**

It was my pleasure to write this thesis to conclude my research in the past four years. I would like to express my gratitude to everyone who helped me in this process. I may not mention all of them because of the limitation. I have to say thank you to my major supervisor Professor Ryo Tanaka, he makes my research possible. He provided me the experiment condition and unselfishness help in life and work.

Also, I would like to express my appreciation to my second and third supervisors associate professor Miki Shimizu from the department of diagnostic imaging at Tokyo University of Agriculture and Technology, and professor Yuji Uzuka from the division of small animals surgery from Iwate University. They helped me with their valuable advice, kindness to finish my work.

Also, I would like to thank professor Ken Takahashi for his help. His professional advice in evaluating IVPG helped me explained some mechanisms that eventually helped me finished my Ph.D. program.

I will express my thanks to my committee member: professor, Yasuo Nambo from Obihiro university of agriculture and veterinary medicine; associate professor, Sanae Shibata from Gifu University and professor, Tsuyoshi Uchide from TUAT, and professor Yuji Uzuka from Iwate university. Thank you for your time and effort to improve the quality of my research.

I would like to express my sincere appreciation to my college including but not limited to Ahmed S. Mandour, Hanan Hendawy, Tomohiko Yoshida, Hussein M. El-Husseiny, Yusuke Ozai, Aki Takeuchi, Akiko Uemura, Ryosuke Namiki, John, and Nukky, and.

Kotomi Sato, Kenjiro Shiraishi, Akira Yairo, and other students and graduates of the member of the department of veterinary surgery for their cooperation. I am also indebted to all the dogs for their silent sacrifice, which was indispensable for success in my study.

Lastly, I would like to thank the Mitsubishi group for providing a scholarship to me, and I would thank everyone I meet in Japan, you guys helped me grow up from a young man to a mature veterinarian. The memory and happiness will always stay at bottom of my heart.

Danfu Ma

April 4<sup>th</sup>, 2021



## References

1. Virani SS, Alonso A, Benjamin EJ, Bittencourt MS, Callaway CW, Carson AP, et al. Heart disease and stroke statistics—2020 update: a report from the American Heart Association. *Circulation*. 2020;141(9):e139-e596.
2. Hoque M, Saxena A, REETU M, BODH G, BODH D. Cardiac diseases in dogs. *Indian Journal of Animal Health* v58. 2019:1-20.
3. Paige CF, Abbott JA, Elvinger F, Pyle RL. Prevalence of cardiomyopathy in apparently healthy cats. *Journal of the American Veterinary Medical Association*. 2009;234(11):1398-403.
4. Fox PR, Keene BW, Lamb K, Schober KA, Chetboul V, Luis Fuentes V, et al. International collaborative study to assess cardiovascular risk and evaluate long - term health in cats with preclinical hypertrophic cardiomyopathy and apparently healthy cats: the REVEAL study. *Journal of veterinary internal medicine*. 2018;32(3):930-43.
5. Ommen SR, Nishimura RA, Appleton CP, Miller F, Oh JK, Redfield MM, et al. Clinical utility of Doppler echocardiography and tissue Doppler imaging in the estimation of left ventricular filling pressures: a comparative simultaneous Doppler-catheterization study. *Circulation*. 2000;102(15):1788-94.
6. Mertens L, Friedberg MK. The gold standard for noninvasive imaging in congenital heart disease: echocardiography. *Current Opinion in Cardiology*. 2009;24(2):119-24.
7. Creager MA. Early intervention in heart failure. *Drugs*. 1990;39 Suppl 4:4-9; discussion 22-4.
8. Schober KE, Hart TM, Stern JA, Li X, Samii VF, Zekas LJ, et al. Detection of Congestive Heart Failure in Dogs by Doppler Echocardiography. *Journal of Veterinary Internal Medicine*. 2010;24(6):1358-68.
9. Falsetti HL, Verani MS, Chen CJ, Cramer JA. Regional pressure differences in the left ventricle. Catheterization and cardiovascular diagnosis. 1980;6(2):123-34.
10. Kim DW, Suh CH, Yoon HM, Kim JR, Jung AY, Lee JS, et al. Visibility of normal appendix on CT, MRI, and sonography: a systematic review and meta-analysis. *American Journal of Roentgenology*. 2018;211(3):W140-W50.
11. Mertens L, Friedberg MK. The gold standard for noninvasive imaging in congenital heart disease: echocardiography. *Current opinion in cardiology*. 2009;24(2):119-24.
12. Boyd AC, Schiller NB, Thomas L. Principles of transthoracic echocardiographic evaluation. *Nature Reviews Cardiology*. 2015;12(7):426-40.
13. Campbell Fa, Kittleson MD. The effect of hydration status on the echocardiographic measurements of normal cats. *Journal of veterinary internal medicine*. 2007;21(5):1008-15.
14. Ling D, Rankin J, Edwards 2nd C, McHale P, Anderson R. Regional diastolic mechanics of the left ventricle in the conscious dog. *American Journal of Physiology-Heart and Circulatory Physiology*. 1979;236(2):H323-H30.
15. Courtois M, Kovacs S, Ludbrook P. Physiological early diastolic intraventricular pressure gradient is lost during acute myocardial ischemia. *Circulation*. 1990;81(5):1688-96.
16. Yotti R, Bermejo J, Antoranz JC, Rojo-Álvarez JL, Allue C, Silva J, et al. Noninvasive assessment of ejection intraventricular pressure gradients. *Journal of the American College of Cardiology*. 2004;43(9):1654-62.
17. Yotti R, Bermejo J, Benito Y, Antoranz JC, Desco MM, Rodríguez-Pérez D, et al. Noninvasive estimation of the rate of relaxation by the analysis of intraventricular pressure gradients. *Circulation: Cardiovascular Imaging*. 2011;4(2):94-104.
18. Yotti R, Bermejo J, Desco MM, Antoranz JC, Rojo-Álvarez JL, Cortina C, et al. Doppler-Derived Ejection Intraventricular Pressure Gradients Provide a Reliable Assessment of Left Ventricular Systolic Chamber Function. *Circulation*. 2005;112(12):1771-9.
19. Popovic ZB, Richards KE, Greenberg NL, Rovner A, Drinko J, Cheng Y, et al. Scaling of diastolic intraventricular pressure gradients is related to filling time duration. *Am J Physiol Heart Circ Physiol*. 2006;291(2):H762-9.
20. Greenberg NL, Vandervoort PM, Firstenberg MS, Garcia MJ, Thomas JD. Estimation of diastolic intraventricular pressure gradients by Doppler M-mode echocardiography. *Am J Physiol Heart Circ Physiol*. 2001;280(6):H2507-15.
21. Kasner M, Westermann D, Steendijk P, Gaub R, Wilkenshoff U, Weitmann K, et al. Utility of Doppler Echocardiography and Tissue Doppler Imaging in the Estimation of Diastolic Function in Heart Failure With Normal Ejection Fraction. *Circulation*. 2007;116(6):637-47.
22. Ie EH, Vletter WB, Folkert J, Nette RW, Weimar W, Roelandt JR, et al. Preload dependence of new Doppler techniques limits their utility for left ventricular diastolic function assessment in hemodialysis patients. *Journal of the American Society of Nephrology*. 2003;14(7):1858-62.

23. Jackson G, Gibbs CR, Davies MK, Lip GY. ABC of heart failure. Pathophysiology. *BMJ*. 2000;320(7228):167-70.
24. Kitpipatkun P, Matsuura K, Shimada K, Uemura A, Goya S, Yoshida T, et al. Key factors of diastolic dysfunction and abnormal left ventricular relaxation in diabetic rats. *J Med Ultrason*. 2020;47(3):347-56.
25. Wallmeyer K, Wann L, Sagar KB, Kalbfleisch J, Klopfenstein H. The influence of preload and heart rate on Doppler echocardiographic indexes of left ventricular performance: comparison with invasive indexes in an experimental preparation. *Circulation*. 1986;74(1):181-6.
26. Hurrell DG, Nishimura RA, Ilstrup DM, Appleton CP. Utility of Preload Alteration in Assessment of Left Ventricular Filling Pressure by Doppler Echocardiography: A Simultaneous Catheterization and Doppler Echocardiographic Study. *Journal of the American College of Cardiology*. 1997;30(2):459-67.
27. Oh JK, Park S-J, Nagueh SF. Established and novel clinical applications of diastolic function assessment by echocardiography. *Circulation: Cardiovascular Imaging*. 2011;4(4):444-55.
28. Maharaj R. Diastolic dysfunction and heart failure with a preserved ejection fraction: Relevance in critical illness and anaesthesia. *J Saudi Heart Assoc*. 2012;24(2):99-121.
29. Cochet A, Quilichini G, Dygai-Cochet I, Touzery C, Toubreau M, Berriolo-Riedinger A, et al. Baseline diastolic dysfunction as a predictive factor of trastuzumab-mediated cardiotoxicity after adjuvant anthracycline therapy in breast cancer. *Breast cancer research and treatment*. 2011;130(3):845-54.
30. Ohara T, Niebel CL, Stewart KC, Charonko JJ, Pu M, Vlachos PP, et al. Loss of adrenergic augmentation of diastolic intra-LV pressure difference in patients with diastolic dysfunction: evaluation by color M-mode echocardiography. *JACC Cardiovasc Imaging*. 2012;5(9):861-70.
31. Iwano H, Kamimura D, Fox E, Hall M, Vlachos P, Little WC. Altered spatial distribution of the diastolic left ventricular pressure difference in heart failure. *J Am Soc Echocardiogr*. 2015;28(5):597-605 e1.
32. Pasipoularides A. Right and left ventricular diastolic flow field: why are measured intraventricular pressure gradients small? *Rev Esp Cardiol*. 2013;66(5):337-41.
33. Palmiero P, Zito A, Maiello M, Cameli M, Modesti PA, Muiesan ML, et al. Left ventricular diastolic function in hypertension: methodological considerations and clinical implications. *J Clin Med Res*. 2015;7(3):137-44.
34. Takahashi K, Nii M, Takigiku K, Toyono M, Iwashima S, Inoue N, et al. Development of suction force during early diastole from the left atrium to the left ventricle in infants, children, and adolescents. *Heart Vessels*. 2019;34(2):296-306.
35. Chung CS, Karamanoglu M, Kovács SJ. Duration of diastole and its phases as a function of heart rate during supine bicycle exercise. *American Journal of Physiology-Heart and Circulatory Physiology*. 2004;287(5):H2003-H8.
36. Barton CH, Ni Z, Vaziri ND. Enhanced nitric oxide inactivation in aortic coarctation-induced hypertension. *Kidney Int*. 2001;60(3):1083-7.
37. Huang J, Wang D, Zheng J, Huang X, Jin H. Hydrogen sulfide attenuates cardiac hypertrophy and fibrosis induced by abdominal aortic coarctation in rats. *Molecular medicine reports*. 2012;5(4):923-8.
38. SAKAI T, MATSUMOTO N, YOSHIDA H, Takaori M. Biodegradation of isoflurane in dogs. *Kawasaki medical journal*. 1988;14(2):97-102.
39. Ismaeil Mohamed S, Tkachenko I, Gamperl Kurt A, Hickey Robert F, Cason Brian A. Mechanisms of Isoflurane-induced Myocardial Preconditioning in Rabbits *Anesthesiology*. 1999;90(3):812-21.
40. Wilson F. Stages of anesthesia. In: Burton VW, Davies AH, Kilpatrick A, McIlmurray MB, Pring JE, Wilson F, editors. *Essential Accident and Emergency Care*. Dordrecht: Springer Netherlands; 1981. p. 212-5.
41. Zacchigna S, Paldino A, Falcão-Pires I, Daskalopoulos EP, Dal Ferro M, Vodret S, et al. Towards standardization of echocardiography for the evaluation of left ventricular function in adult rodents: a position paper of the ESC Working Group on Myocardial Function. *Cardiovascular research*. 2021;117(1):43-59.
42. Previtali M, Chieffo E, Ferrario M, Klersy C. Is mitral E/E' ratio a reliable predictor of left ventricular diastolic pressures in patients without heart failure? *European Heart Journal–Cardiovascular Imaging*. 2012;13(7):588-95.
43. Kuroda K, Kato TS, Amano A. Hypertensive cardiomyopathy: A clinical approach and literature review. *World J Hypertens*. 2015; 5(2): 41-52.
44. Chung CS, Afonso L. Heart Rate Is an Important Consideration for Cardiac Imaging of Diastolic Function. *JACC Cardiovasc Imaging*. 2016;9(6):756-8.
45. Palatini P. Role of elevated heart rate in the development of cardiovascular disease in hypertension. *Hypertension*. 2011;58(5):745-50.
46. Huang J, Wang D, Zheng J, Huang X, Jin H. Hydrogen sulfide attenuates cardiac hypertrophy and fibrosis induced by abdominal aortic coarctation in rats. *Mol Med Rep*. 2012;5(4):923-8.
47. Chung CS, Kovacs SJ. Consequences of increasing heart rate on deceleration time, the velocity-time integral, and E/A. *Am J Cardiol*. 2006;97(1):130-6.

48. Previtali M, Chieffo E, Ferrario M, Klersy C. Is mitral E/E' ratio a reliable predictor of left ventricular diastolic pressures in patients without heart failure? *European Heart Journal - Cardiovascular Imaging*. 2011;13(7):588-95.
49. Frohlich ED, Susic D. Pressure overload. *Heart failure clinics*. 2012;8(1):21-32.
50. Kuroda K, Kato TS, Amano A. Hypertensive cardiomyopathy: A clinical approach and literature review. *World J Hypertens*. 2015;5(2):41-52.
51. Drazner MH. The progression of hypertensive heart disease. *Circulation*. 2011;123(3):327-34.
52. Crozatier B, Ventura-clapier RJC. Is Inhibition of Hypertrophy a Good Therapeutic Strategy in Ventricular Pressure Overload?: Inhibition of Hypertrophy, Per Se, May Not Be a Good Therapeutic Strategy in Ventricular Pressure Overload. *Circulation*. 2015;131(16):1448-57.
53. Yum B, Archambault A, Levitan EB, Dharamdasani T, Kneifati-Hayek J, Hanlon JT, et al. Indications for beta-Blocker Prescriptions in Heart Failure with Preserved Ejection Fraction. *J Am Geriatr Soc*. 2019;67(7):1461-6.
54. Silverman DN, Plante TB, Infeld M, Callas PW, Juraschek SP, Dougherty GB, et al. Association of beta-Blocker Use With Heart Failure Hospitalizations and Cardiovascular Disease Mortality Among Patients With Heart Failure With a Preserved Ejection Fraction: A Secondary Analysis of the TOPCAT Trial. *JAMA Netw Open*. 2019;2(12):e1916598.
55. Oláh A, Németh BT, Mátyás C, Hidi L, Lux Á, Ruppert M, et al. Physiological and pathological left ventricular hypertrophy of comparable degree is associated with characteristic differences of in vivo hemodynamics. *American Journal of Physiology-Heart and Circulatory Physiology*. 2016;310(5):H587-H97.
56. Ruppert M, Korkmaz-Icöz S, Li S, Merkely B, Karck M, Radovits T, et al. Reverse electrical remodeling following pressure unloading in a rat model of hypertension-induced left ventricular myocardial hypertrophy. *Hypertension Research*. 2017;40(7):637-45.
57. Wang J, Xiong X, Feng B. Cardiovascular effects of salvianolic acid B. *Evidence-Based Complementary and Alternative Medicine*. 2013;2013.
58. Lv Z, Xu L. Salvianolic acid B inhibits ERK and p38 MAPK signaling in TGF-1-stimulated human hepatic stellate cell line (LX-2) via distinct pathways. *Evidence-Based Complementary and Alternative Medicine*. 2012;2012.
59. Lu Y, Zheng Y, Liu X, Liang X, Ngai S, Li T, et al. Metabolomic profiles of myocardial ischemia under treatment with salvianolic acid B. *Chin Med*. 2012;7(1):6.
60. Bermejo J, Antoranz JC, Yotti R, Moreno M, Garcia-Fernandez MA. Spatio-temporal mapping of intracardiac pressure gradients. A solution to Euler's equation from digital postprocessing of color Doppler M-mode echocardiograms. *Ultrasound Med Biol*. 2001;27(5):621-30.
61. Stewart KC, Kumar R, Charonko JJ, Ohara T, Vlachos PP, Little WC. Evaluation of LV diastolic function from color M-mode echocardiography. *JACC Cardiovasc Imaging*. 2011;4(1):37-46.
62. Notomi Y, Popovic ZB, Yamada H, Wallick DW, Martin MG, Oryszak SJ, et al. Ventricular untwisting: a temporal link between left ventricular relaxation and suction. *Am J Physiol Heart Circ Physiol*. 2008;294(1):H505-13.
63. Ohara T, Niebel CL, Stewart KC, Charonko JJ, Pu M, Vlachos PP, et al. Loss of adrenergic augmentation of diastolic intra-LV pressure difference in patients with diastolic dysfunction: evaluation by color M-mode echocardiography. *JACC Cardiovasc Imaging*. 2012;5(9):861-70.
64. Kobayashi M, Takahashi K, Yamada M, Yazaki K, Matsui K, Tanaka N, et al. Assessment of early diastolic intraventricular pressure gradient in the left ventricle among patients with repaired tetralogy of Fallot. *Heart Vessels*. 2017;32(11):1364-74.
65. Rovner A, Smith R, Greenberg NL, Tuzcu EM, Smedira N, Lever HM, et al. Improvement in diastolic intraventricular pressure gradients in patients with HOCM after ethanol septal reduction. *Am J Physiol Heart Circ Physiol*. 2003;285(6):H2492-9.
66. Fan Z, Gao Y, Huang Z, Xue F, Wu S, Yang J, et al. Protective effect of hydrogen-rich saline on pressure overload-induced cardiac hypertrophy in rats: possible role of JAK-STAT signaling. *BMC cardiovascular disorders*. 2018;18(1):1-7.
67. Iwano H, Kamimura D, Fox E, Hall M, Vlachos P, Little WC. Altered spatial distribution of the diastolic left ventricular pressure difference in heart failure. *J Am Soc Echocardiogr*. 2015;28(5):597-605 e1.
68. Kai H, Kuwahara F, Tokuda K, Imaizumi TJHr. Diastolic dysfunction in hypertensive hearts: roles of perivascular inflammation and reactive myocardial fibrosis. 2005;28(6):483.
69. Wang S, Xue H, Zou Y, Sun K, Fu C, Wang H, et al. Left ventricular hypertrophy, abnormal ventricular geometry and relative wall thickness are associated with increased risk of stroke in hypertensive patients among the Han Chinese. *Hypertension Research*. 2014;37(9):870-4.
70. Kuwahara F, Kai H, Tokuda K, Kai M, Takeshita A, Egashira K, et al. Transforming growth factor-β function blocking prevents myocardial fibrosis and diastolic dysfunction in pressure-overloaded rats. 2002;106(1):130-5.

71. Ni M, Yang Z-W, Li D-J, Li Q, Zhang S-H, Su D-F, et al. A potential role of alpha-7 nicotinic acetylcholine receptor in cardiac angiogenesis in a pressure-overload rat model. *Journal of pharmacological sciences*. 2010;114(3):311-9.
72. Dai C, Li Q, May HI, Li C, Zhang G, Sharma G, et al. Lactate Dehydrogenase A Governs Cardiac Hypertrophic Growth in Response to Hemodynamic Stress. *Cell reports*. 2020;32(9):108087.
73. Yu J, Chen R, Tan Y, Wu J, Qi J, Zhang M, et al. Salvianolic acid B alleviates heart failure by inactivating ERK1/2/GATA4 signaling pathway after pressure overload in mice. 2016;11(11):e0166560.
74. Bachner-Hinzen N, Ertracht O, Leitman M, Vered Z, Shimoni S, Beerli R, et al. Layer-specific strain analysis by speckle tracking echocardiography reveals differences in left ventricular function between rats and humans. 2010;299(3):H664-H72.
75. Popovic ZB, Richards KE, Greenberg NL, Rovner A, Drinko J, Cheng Y, et al. Scaling of diastolic intraventricular pressure gradients is related to filling time duration. *Am J Physiol-Heart C*. 2006;291(2):H762-9.
76. Silverman DN, Plante TB, Infeld M, Callas PW, Juraschek SP, Dougherty GB, et al. Association of  $\beta$ -Blocker Use With Heart Failure Hospitalizations and Cardiovascular Disease Mortality Among Patients With Heart Failure With a Preserved Ejection Fraction: A Secondary Analysis of the TOPCAT Trial. *JAMA Network Open*. 2019;2(12):e1916598-e.
77. Bergström A, Andersson B, Edner M, Nylander E, Persson H, Dahlström U. Effect of carvedilol on diastolic function in patients with diastolic heart failure and preserved systolic function. Results of the Swedish Doppler - echocardiographic study (SWEDIC). *European journal of heart failure*. 2004;6(4):453-61.
78. Edelmann F, Musial-Bright L, Gelbrich G, Trippel T, Radenovic S, Wachter R, et al. Tolerability and feasibility of beta-blocker titration in HFpEF versus HFrEF: insights from the CIBIS-ELD trial. *JACC: Heart Failure*. 2016;4(2):140-9.
79. Cotrim C, Lopes LR, Almeida AR, Miranda R, Almeida AG, Cotrim H, et al. Efficacy of beta-blocker therapy in symptomatic athletes with exercise-induced intra-ventricular gradients. *Cardiovasc Ultrasound*. 2010;8(1):38.
80. Qiao Z, Xu Y. Salvianolic Acid B Alleviating Myocardium Injury in Ischemia Reperfusion Rats. *Afr J Tradit Complement Altern Med*. 2016;13(4):157-61.
81. Yamamoto K, Masuyama T, Sakata Y, Nishikawa N, Mano T, Yoshida J, et al. Myocardial stiffness is determined by ventricular fibrosis, but not by compensatory or excessive hypertrophy in hypertensive heart. 2002;55(1):76-82.
82. Gao H, Bo Z, Wang Q, Luo L, Zhu H, Ren Y. Salvianic acid B inhibits myocardial fibrosis through regulating TGF- $\beta$ 1/Smad signaling pathway. *Biomedicine & Pharmacotherapy*. 2019;110:685-91.
83. Wang C, Luo H, Xu Y, Tao L, Chang C, Shen X. Salvianolic Acid B-Alleviated Angiotensin II Induces Cardiac Fibrosis by Suppressing NF- $\kappa$ B Pathway In Vitro. *Med Sci Monit*. 2018;24:7654-64.
84. Qiu H, Liu W, Lan T, Pan W, Chen X, Wu H, et al. Salvianolate reduces atrial fibrillation through suppressing atrial interstitial fibrosis by inhibiting TGF- $\beta$ 1/Smad2/3 and TXNIP/NLRP3 inflammasome signaling pathways in post-MI rats. 2018;51:255-65.
85. Molkentin JD, Jochheim BC. The zinc finger-containing transcription factors GATA-4, -5, and -6 ubiquitously expressed regulators of tissue-specific gene expression. 2000;275(50):38949-52.
86. Bernardo BC, Weeks KL, Pretorius L, McMullen JR, et al. Molecular distinction between physiological and pathological cardiac hypertrophy: experimental findings and therapeutic strategies. 2010;128(1):191-227.
87. Suzuki R, Mochizuki Y, Yuchi Y, Yasumura Y, Saito T, Teshima T, et al. Assessment of myocardial function in obstructive hypertrophic cardiomyopathy cats with and without response to medical treatment by carvedilol. *BMC Vet Res*. 2019;15(1):376-.
88. Yan Y-Y, Yang Y-H, Wang W-W, Pan Y-T, Zhan S-Y, Sun M-Y, et al. Post-marketing safety surveillance of the *Salvia miltiorrhiza* Dipsacaceae Salt for infusion: a real world study. *PloS one*. 2017;12(1):e0170182.
89. Ammirati E, Contri R, Coppini R, Cecchi F, Frigerio M, Olivetto I. Pharmacological treatment of hypertrophic cardiomyopathy: current practice and novel perspectives. *European journal of heart failure*. 2016;18(9):1106-18.
90. Parfrey P, Foley R, Harnett J, Kent G, Murray D, Barre P. Outcome and risk factors for left ventricular disorders in chronic uraemia. *Nephrology Dialysis Transplantation*. 1996;11(7):1277-85.
91. Hung S-C, Kuo K-L, Peng C-H, Wu C-H, Lien Y-C, Wang Y-C, et al. Volume overload correlates with cardiovascular risk factors in patients with chronic kidney disease. *Kidney international*. 2014;85(3):703-9.
92. Alhaj E, Alhaj N, Rahman I, Niazi TO, Berkowitz R, Klapholz M. Uremic cardiomyopathy: an underdiagnosed disease. *Congestive heart failure*. 2013;19(4):E40-E5.
93. Kim HJ, Moradi H, Yuan J, Norris K, Vaziri ND. Renal mass reduction results in accumulation of lipids and dysregulation of lipid regulatory proteins in the remnant kidney. *American Journal of Physiology-Renal Physiology*. 2009;296(6):F1297-F306.



94. Gong W, Mao S, Yu J, Song J, Jia Z, Huang S, et al. NLRP3 deletion protects against renal fibrosis and attenuates mitochondrial abnormality in mouse with 5/6 nephrectomy. *American Journal of Physiology-Renal Physiology*. 2016;310(10):F1081-F8.
95. Kostis JB, Shelton B, Gosselin G, Goulet C, Hood WB, Jr., Kohn RM, et al. Adverse effects of enalapril in the Studies of Left Ventricular Dysfunction (SOLVD). SOLVD Investigators. *Am Heart J*. 1996;131(2):350-5.
96. Wu P, Yan Y, Ma L-l, Hou B-y, He Y-y, Zhang L, et al. Effects of the Nrf2 protein modulator salvianolic acid A alone or combined with metformin on diabetes-associated macrovascular and renal injury. *Journal of Biological Chemistry*. 2016;291(42):22288-301.
97. Tongqiang L, Shaopeng L, Xiaofang Y, Nana S, Xialian X, Jiachang H, et al. Salvianolic Acid B Prevents Iodinated Contrast Media-Induced Acute Renal Injury in Rats via the PI3K/Akt/Nrf2 Pathway. *Oxidative Medicine and Cellular Longevity*. 2016;2016:7079487.
98. Li J, Zhang C, He W, Qiao H, Chen J, Wang K, et al. Coordination-driven assembly of catechol-modified chitosan for the kidney-specific delivery of salvianolic acid B to treat renal fibrosis. *Biomaterials science*. 2018;6(1):179-88.
99. He Y, Lu R, Wu J, Pang Y, Li J, Chen J, et al. Salvianolic acid B attenuates epithelial-mesenchymal transition in renal fibrosis rats through activating Sirt1-mediated autophagy. *Biomedicine & Pharmacotherapy*. 2020;128:110241.
100. Watson LE, Sheth M, Denyer RF, Dostal DE. Baseline echocardiographic values for adult male rats. *Journal of the American Society of Echocardiography*. 2004;17(2):161-7.
101. Khan Z, Pandey M. Role of kidney biomarkers of chronic kidney disease: An update. *Saudi journal of biological sciences*. 2014;21(4):294-9.
102. Gava AL, Freitas FP, Balarini CM, Vasquez EC, Meyrelles SS. Effects of 5/6 nephrectomy on renal function and blood pressure in mice. *International journal of physiology, pathophysiology and pharmacology*. 2012;4(3):167.
103. Santos LS, Chin EWK, Ioshii SO, Tambara Filho R. Surgical reduction of the renal mass in rats: morphologic and functional analysis on the remnant kidney. *Acta cirurgica brasileira*. 2006;21(4):252-7.
104. Nauta JF, Hummel YM, Tromp J, Ouwerkerk W, van der Meer P, Jin X, et al. Concentric vs. eccentric remodelling in heart failure with reduced ejection fraction: clinical characteristics, pathophysiology and response to treatment. *European journal of heart failure*. 2020;22(7):1147-55.
105. Xu Q, Dalic A, Fang L, Kiriazis H, Ritchie RH, Sim K, et al. Myocardial oxidative stress contributes to transgenic  $\beta_2$ -adrenoceptor activation-induced cardiomyopathy and heart failure. *Br J Pharmacol*. 2011;162(5):1012-28.
106. Zhao M, Fajardo G, Urashima T, Spin JM, Poorfarahani S, Rajagopalan V, et al. Cardiac pressure overload hypertrophy is differentially regulated by  $\beta$ -adrenergic receptor subtypes. *American Journal of Physiology-Heart and Circulatory Physiology*. 2011;301(4):H1461-H70.
107. Ma D, Mandour AS, Yoshida T, Matsuura K, Shimada K, Kitpipatkun P, et al. Intraventricular pressure gradients change during the development of left ventricular hypertrophy: Effect of salvianolic acid B and beta-blocker. *Ultrasound*. 2021;1742271X20987584.
108. Wang X, Shapiro JL. Evolving concepts in the pathogenesis of uraemic cardiomyopathy. *Nature Reviews Nephrology*. 2019;15(3):159-75.
109. Wang C, Luo H, Xu Y, Tao L, Chang C, Shen X. Salvianolic acid B-alleviated angiotensin II induces cardiac fibrosis by suppressing NF- $\kappa$ B pathway in vitro. *Medical science monitor: international medical journal of experimental and clinical research*. 2018;24:7654.
110. Chinali M, Matteucci MC, Franceschini A, Doyon A, Pongiglione G, Rinelli G, et al. Advanced Parameters of Cardiac Mechanics in Children with CKD: The 4C Study. *Clinical Journal of the American Society of Nephrology*. 2015;10(8):1357-63.
111. Winterberg PD, Jiang R, Maxwell JT, Wang B, Wagner MB. Myocardial dysfunction occurs prior to changes in ventricular geometry in mice with chronic kidney disease (CKD). *Physiological reports*. 2016;4(5):e12732.
112. Böhm M, Swedberg K, Komajda M, Borer JS, Ford I, Dubost-Brama A, et al. Heart rate as a risk factor in chronic heart failure (SHIFT): the association between heart rate and outcomes in a randomised placebo-controlled trial. *The Lancet*. 2010;376(9744):886-94.
113. Nagueh SF, Smiseth OA, Appleton CP, Byrd BF, Dokainish H, Edvardsen T, et al. Recommendations for the evaluation of left ventricular diastolic function by echocardiography: an update from the American Society of Echocardiography and the European Association of Cardiovascular Imaging. *European Journal of Echocardiography*. 2016;17(12):1321-60.
114. Muhl C, Dassen WRM, Kuipers H. Cardiac remodelling: concentric versus eccentric hypertrophy in strength and endurance athletes. *Neth Heart J*. 2008;16(4):129-33.